A Chemically-Responsive *bis*-Acridinium Receptor

A. Gosset,[a] Z. Xu,[a] F. Maurel,*[a] L.-M. Chamoreau,[b] S. Nowak,[a] G. Vives,[b] C. Perruchot,[a] V. Heitz*[c] and H.-P. Jacquot de Rouville*[a,c]

[a]Univ Paris Diderot, Sorbonne Paris Cite, ITODYS, UMR CNRS 7086, 15 rue J-A de Baif, 75013 Paris, France
E-mail : maurel@univ-paris-diderot.fr
E-mail : h-p.jacquot@univ-paris-diderot.fr
[b]Sorbonne Universités, UPMC Univ Paris 06, UMR 8232, Institut Parisien de Chimie Moléculaire, 4 place Jussieu, 75005, Paris, France.
[c]Laboratoire de Synthèse des Assemblages Moléculaires Multifonctionnels, Institut de Chimie de Strasbourg, CNRS/UMR 7177, 4, rue Blaise Pascal, 67000 Strasbourg, France
E-mail : vheitz@univ-paris-diderot.fr
E-mail : hpjacquot@univ-paris-diderot.fr

Supporting Information

Table of Contents

1. Material and Methods

Synthesis. Materials, syntheses and general procedures of the target molecule **1.2PF$_6$**, including 10-methyl-9(10H)-acridone[S1] and 1,3-bis(4,4,5,5-tetramethyl-1,3,2-dioxaborolan-2-yl)benzene (**2**)[S2], are provided in the Supporting Information. All compounds were synthesized using schlenk technics and were fully characterized by 1D (^{1}H, ^{13}C{^{1}H}, ^{31}P{^{1}H} and ^{19}F{^{1}H}) and 2D (COSY, HSQC and HMBC) NMR experiments and by mass spectrometry experiments. NMR experiments were monitored at 400 MHz, on a *Bruker Advance III 400* at 298 K unless specified by other means. Variable temperature experiments were monitored at 600 MHz, *Bruker Advance III 600.*

Crystallographic Method. A single crystal of the compound was selected, mounted onto a cryoloop, and transferred in a cold nitrogen gas stream. Intensity data were collected with a BRUKER Kappa-APEXII diffractometer with graphite-monochromated Mo-Kα radiation (λ = 0.71073 Å). Data collection were performed with APEX2 suite (BRUKER). Unit-cell parameters refinement, integration and data reduction were carried out with SAINT program (BRUKER). SADABS (BRUKER) was used for scaling and multi-scan absorption corrections. In the WinGX suite of programs,[S3] the structure was solved with ShelxT[S4] program and refined by full-matrix least-squares methods using SHELXL-14.[S5] All non-hydrogen atoms were refined anisotropically. Hydrogen atoms were placed at calculated positions and refined with a riding model. A model of disorder was introduced for a PF_6^- anion and for an acetonitrile molecule.

Computational Method. The inability of DFT method to correctly account for dispersive interactions is well known. This problem is due to the fact that dispersion forces result from long-range correlations between electrons, whereas some of the current exchange-correlation potentials model only local correlation effects. Several improvements to correct the drawbacks of first functionals have been proposed. We used in this paper the long range corrected ωB97XD functional that allow an accurate description of systems involving noncovalent interactions with strong dispersion effects with a moderate computational cost. All ab initio simulations have been achieved with the GAUSSIAN09 program, applying default procedures, integration grids, algorithms and parameters, except when noted. The geometries of the studied compounds were optimized using both the ωB97XD hybrid exchange correlation functional and the standard 6-31G* basis set. We have systematically computed the vibrational spectrum on the minimized

structures to check that there is no imaginary vibrational mode. The complexation energies between 1 and TTF have been estimated by energy difference between the complex and the sum of the isolated constituents. The complexation energy was corrected from the basis set superposition errors (BSSE) using the standard counterpoise (CP) approach. The modelling of bulk solvent effects (here acetonitrile, as in the experiments) is included through the Polarizable Continuum Model (PCM) [PCM]. The accuracy of the different DFT functionals (such as PBE0, BLYP, CAM-B3LYP, HSEH1PBE, LC-ωPBE, ωB97XD, M06 and M062X) for the optical properties have been explored by performing benchmark calculations for 10-methyl-9-phenylacridinium in an water environment and the calculated absorption energies are summarized in Table S6.2 of the ESI. As can be seen from Table S6.2 (ESI), the M06 method gives the absorption energies in excellent agreement with experiment. Hence, the MO6 functional was used to calculate the lowest singlet transitions from the optimized geometry calculated with ωB97XD for all the studied compounds.

2. Synthesis

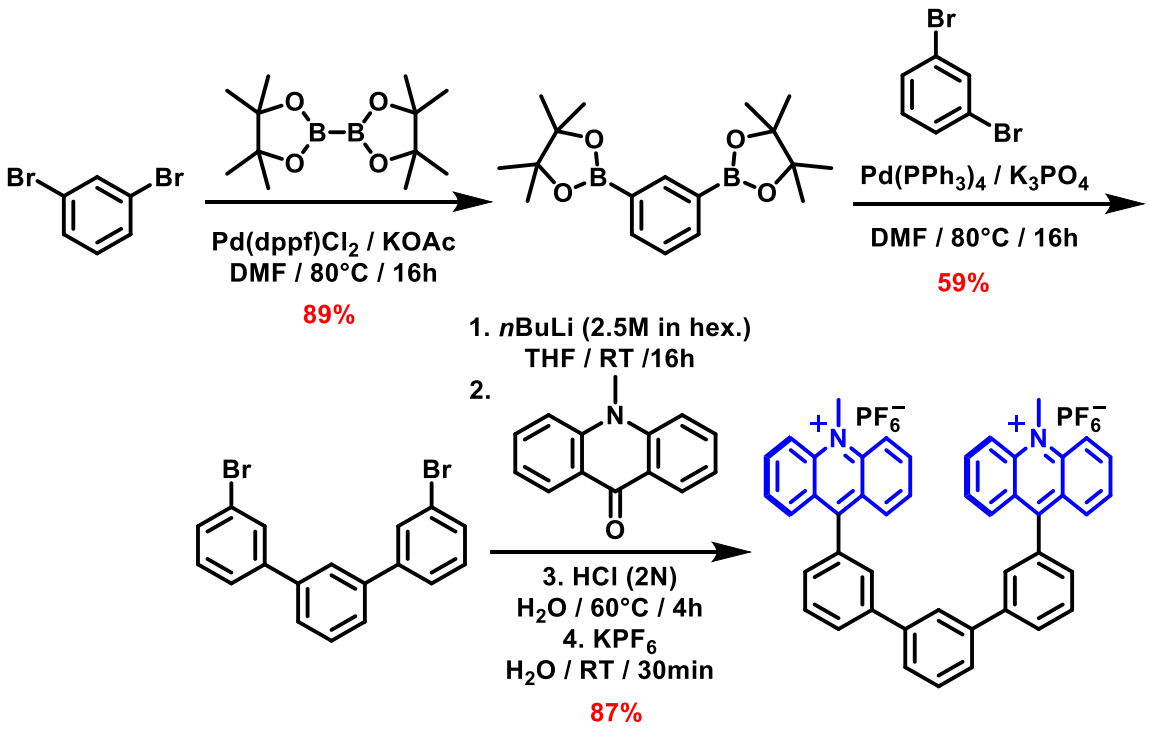

Figure S2.1: Synthesis of **1.2PF6** from 1,3-dibromobenzene.

10-methyl-9(10H)-acridone

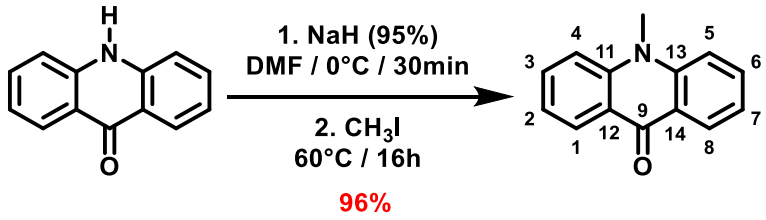

To a solution of 9(10H)-acridanone (976 mg, 5.0 mmol, 1 eq.) in dry DMF (40mL), was added NaH (95% in oil, 300 mg, 12.5 mmol, 2.5 eq.) at 0°C. After 30 min, MeI (0.780 mL, 12.5 mmol, 2.5 eq.) was added and the mixture was stirred at 60°C for 16 hours. The solution was poored into H_2O (400 mL) and the precipitate was filtered. After evaporation of the solvents, the desired product was obtained as a yellowish solid in 96 % yield (1.01 g). ^{1}H NMR (400 MHz, $CDCl_3$, 298 K): δ (ppm) = 8.58 (dd, J = 8.0, 1.5 Hz, 2H, $H_{1/8}$), 7.73 (ddd, J = 8.5, 7.0, 1.5 Hz, 2H, $H_{2/7}$), 7.54 (dd, J = 8.5, 1.0 Hz, 2H, $H_{4/5}$), 7.30 (ddd, J = 8.0, 7.0, 1.0 Hz, 2H, $H_{3/6}$), 3.91 (s, 3H, Me). ^{13}C{^{1}H} NMR (100 MHz, $CDCl_3$, 298 K): δ (ppm) = 178.0 (s, C_9), 142.6 (s, C_{11}), 133.8 (s, $C_{2/7}$), 127.8 (s, $C_{1/8}$), 122.5 (s, C_{12}), 121.2 (s, $C_{3/6}$), 114.7 (s, $C_{4/5}$), 33.6 (s, Me). NMR data are consistent with literature.[1]

1,3-*bis*(4,4,5,5-tetramethyl-1,3,2-dioxaborolan-2-yl)benzene (2)

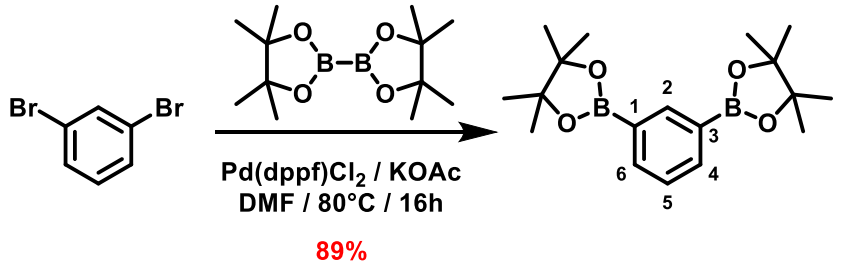

To a degassed solution of 1,3-dibromobenzene (1 g, 4.2 mmol, 1 eq.), *bis*(pinacolato)diboron (2.70 g, 10.6 mmol, 2.5 eq.) and KOAc (2.5 g, 25.4 mmol, 6 eq.) in dry DMF (20 mL), was added $Pd(dppf)Cl_2$ (310 mg, 0.4 mmol, 10%). The reaction mixture was stirred at 80°C for 16 hours. After evaporation of the solvents, the crude product was purified by column chromatography (SiO_2, Petroleum Ether/AcOEt – 9:1), affording the desired product as a colorless oil which crystallizes in 89 % yield (1.24 g). ^{1}H NMR (400 MHz, $CDCl_3$, 298 K): δ (ppm) = 8.28 (d, J = 1.0 Hz, 1H, H_2), 7.90 (dd, J = 7.5, 1.0 Hz, 2H, $H_{4/6}$), 7.37 (td, J = 7.5, 1.0 Hz, 1H, H_5), 1.34 (s, 24H, Me). $^{13}C\{^1H\}$ NMR (100 MHz, $CDCl_3$, 298 K): δ (ppm) = 141.23 (s, C_2), 137.62 (s, $C_{4/6}$), 127.03 (s, C_5), 83.72 (s), 83.48 (s), 24.87 (s, Me). MS (EI): for $C_{18}H_{28}B_2O_4$, m/z_{calc} = 330.2, m/z_{found} = 330.1 (100%, $[M]^+$). Data are consistent with literature.[2]

3,3''-dibromo-1,1':3',1''-terphenyl (3)

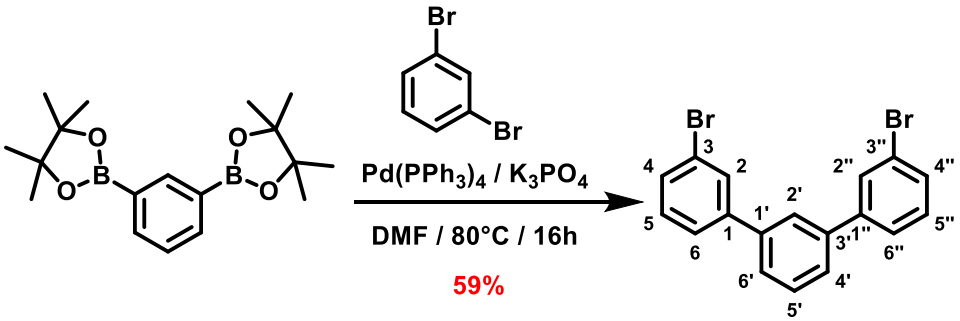

To a degassed solution of 1,3-*bis*(4,4,5,5-tetramethyl-1,3,2-dioxaborolan-2-yl)benzene (200 mg, 0.61 mmol, 1 eq.), 1,3-dibromobenzene (220 µL, 1.82 mmol, 3 eq.) and K_3PO_4 (386 mg, 1.82 mmol, 3 eq.) in DMF (20 mL), was added $Pd(PPh_3)_4$ (140 mg, 0,12 mmol, 20%). The reaction mixture was stirred at 80°C for 16 hours. After evaporation of the solvents, the crude product was purified by column chromatography (SiO_2, Petroleum Ether), affording the desired product as a colorless oil which crystallizes in 51% yield (120 mg). ^{1}H NMR (400 MHz, $CDCl_3$, 298 K): δ (ppm) = 7.78 (t, J = 2.0 Hz, 2H, $H_{2/2''}$), 7.71 (td, J = 2.0, 1.0 Hz, 1H, $H_{2'}$), 7.59 – 7.49 (m, 7H), 7.33 (t, J = 8.0 Hz, 2H, $H_{5/5''}$).$^{13}C\{^1H\}$ NMR (100 MHz, $CDCl_3$, 298 K): δ (ppm) =

143.0 (s), 140.4 (s), 130.4 (s), 130.3 (s, $C_{5/5''}$), 130.2 (s, $C_{2/2''}$), 129.4 (s), 126.6 (s, $C_{2'}$), 125.9 (s), 125.8 (s), 122.9 (s). MS (EI): for $C_{18}H_{12}Br_2$, m/z_{calc} = 385.9, m/z_{found} = 385.8 (100%, $[M]^+$).

Molecular Receptor (1.2PF$_6$)

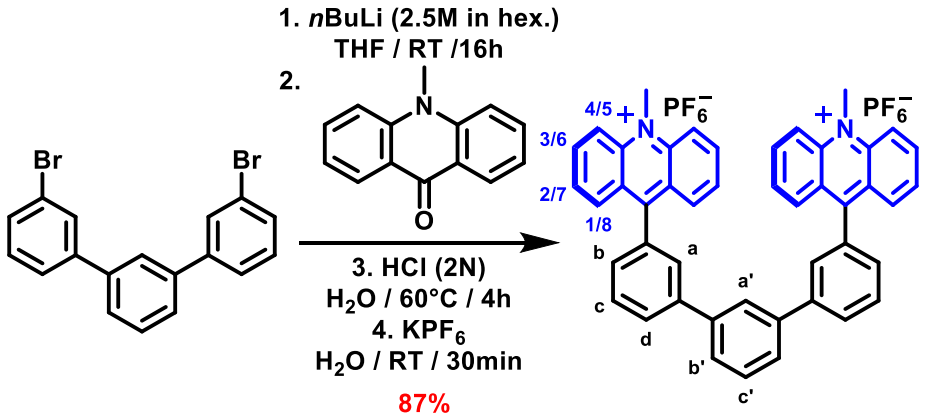

To a solution of 3,3"-dibromo-1,1':3',1"-terphenyl (119 mg, 0.30 mmol, 1 eq.) in dry THF (30 mL), was added dropwise at -78°C a solution of *n*-BuLi (2.5 M in hexanes, 0.244 mL, 0.60 mmol, 2 eq.). After 20 minutes at -78°C, 10-methyl-9(10H)-acridone (128 mg, 0.60 mmol, 2 eq.) was added dropwise. The mixture was further stirred at -78°C for 2 hours, and allowed to room temperature overnight. After addition of a 2N aqueous solution of HCl (30 mL), the reaction mixture was stirred at 60°C for 30min. The aqueous layer was extracted with CH_2Cl_2 (3 x 30 mL), further concentrated and poored into an aqueous solution of KPF_6 (6g in 150 mL). After filtration, the desired product was isolated as a yellow oil in 87% yield (238 mg). ^{1}H NMR (400 MHz, CD_3CN, 298 K): δ (ppm) = 8.62 (d, J = 9.0 Hz, 4H, $H_{4/5}$), 8.38 (ddd, J = 9.0, 7.0, 1.5 Hz, 4H, $H_{3/6}$), 8.12 – 8.08 (m, 6H, $H_{1/8\text{-}b'}$), 8.07 (t, J = 1.5 Hz, 1H, $H_{a'}$), 7.87 (t, J = 1.5 Hz, 2H, H_a), 7.86 – 7.81 (m, 6H, $H_{2/7\text{-}c}$), 7.79 (dd, J = 7.5, 1.5 Hz, 2H, H_d), 7.61 (t, J = 7.5 Hz, 1H, $H_{c'}$), 7.52 (ddd, J = 7.5, 1.5, 1.0 Hz, 2H, H_b), 4.85 (s, 6H, Me). $^{13}C\{^1H\}$ NMR (100 MHz, CD_3CN, 298 K): δ (ppm) = 162.4 (s, $C_{11/14}$), 142.6 (s, C_9), 142.0 (s), 141.4 (s), 139.7 (s, $C_{3/6}$), 134.9 (s), 131.3 (s, $C_{1/8}$), 130.9 (s, $C_{c'}$), 130.5 (s, C_b), 130.2 (s), 129.7 (s), 129.4 (s), 128.8 (s, $C_{2/7}$), 127.9 (s, C_d), 127.1 (s, $C_{a'}$), 127.0 (s, $C_{12/13}$), 119.4 (s, $C_{4/5}$), 39.8 (s, N-Me). $^{19}F\{^1H\}$ NMR (376 MHz, CD_3CN, 298 K): δ (ppm) = –73.05 (d, J = 705 Hz). $^{31}P\{^1H\}$ NMR (162 MHz, CD_3CN, 298 K): δ (ppm) = –144.6 (sept, J = 705 Hz). HRMS (ESI): for $C_{46}H_{34}N_2F_6P$, m/z_{calc} = 759.2358, m/z_{found} = 759.2364 (86%, $[M+PF_6]^+$). UV/Vis (CH_3CN, 298 K): λmax (nm) (ε (L.mol^{-1}.cm^{-1})) = 360 (3100), 409 (1100), 426 (1200), 450 (820). Crystal data for **1.2PF$_6$**: $C_{46}H_{34}N_2$,2(PF_6),2(C_2H_3N), yellow needle, crystal size 0.25 x 0.12 x 0.11 mm^3, triclinic, space group P–1, a = 7.9128(6) Å; b = 16.8566(1) Å; c = 17.3103(1) Å; α = 88.592(2)°; β = 88.414 (2)° ; γ = 82.929(2)°; V = 2289.94 Å^3, Z = 2, ρ_{calcd} = 1.432 , T = 200(2) K, $R1(F2 > 2\sigma F2)$ = 0.0470, $wR2$ = 0.1289. Out of 78626 reflection a total of 13455 were unique. Crystallographic data (excluding structure factors) for the structures reported in this communication have been deposited with the Cambridge Crystallographic Data Center as supplementary publication no. CCDC–1560847.

***bis*-acridane tweezer shaped switch (4)**

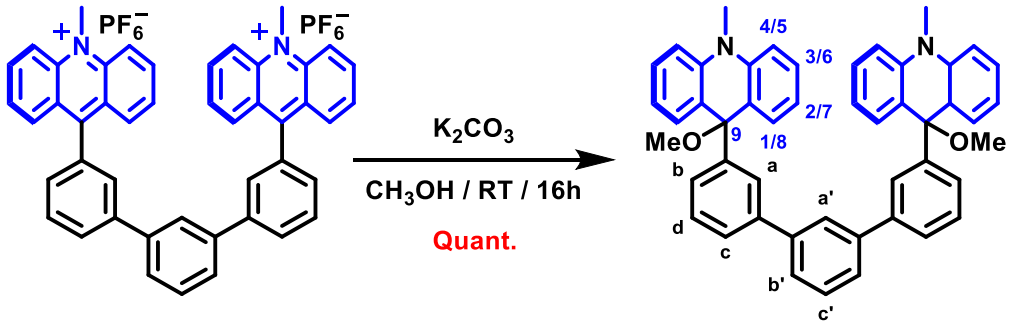

To a solution of **1.2PF6** (50 mg, 55 µmol, 1 eq) in dry CH_3CN (2.5 mL), was added K_2CO_3 (25 mg, 0.18 mmol, 3.3 eq) and dry CH_3OH (0.25 mL). The solution was stirred at room temperature for 16h. After addition of H_2O (30 mL), the reaction mixture, the aqueous layer was extracted with $CHCl_3$ (3 x 30 mL) and dried ($MgSO_4$). The desired product **4** was isolated as a colorless solid in quantitative yield (33 mg). ^{1}H NMR (400 MHz, CD_3CN, 298 K): δ (ppm) = 7.74 (t, J = 1.5 Hz, 2H, H_a), 7.67 (t, J = 1.5 Hz, 1H, $H_{a'}$), 7.47 – 7.37 (m, 6H), 7.35 (dd, J = 8.0, 1.5 Hz, 2H), 7.35 (dd, J = 8.0, 1.5 Hz, 4H, $H_{2/7}$), 7.31 – 7.27 (m, 7H, $H_{4/5}$), 7.24 – 7.19 (m, 2H, H_d), 7.05 (d, J = 7.8 Hz, 4H, $H_{1/8}$), 6.99 – 6.89 (m, 4H, $H_{3/6}$), 3.55 (s, 6H, N-Me), 3.01 (s, 6H, OMe). $^{13}C\{^1H\}$ NMR (100 MHz, CD_3CN, 298 K): δ (ppm) = 150.0 (s), 141.9 (s), 141.0 (s), 140.5 (s), 129.4 (s, $C_{2/7}$), 128.8 (s), 128.4 (s, $C_{4/5}$), 128.1 (s), 126.1 (s), 125.8 (s, $C_{a'}$), 125.2 (s), 124.7 (s), 124.4 (s, C_a), 120.2 (s, $C_{3/6}$), 112.2 (s, $C_{1/8}$), 78.5 (s, C9), 51.1 (s, N-Me), 33.5 (s, OMe). UV/Vis (CH_3CN, 298 K): λmax (nm) (ε (L.mol^{-1}.cm^{-1})) = 275 (30300), 310 (9500), 326 (7600).

3. Structural Characterizations

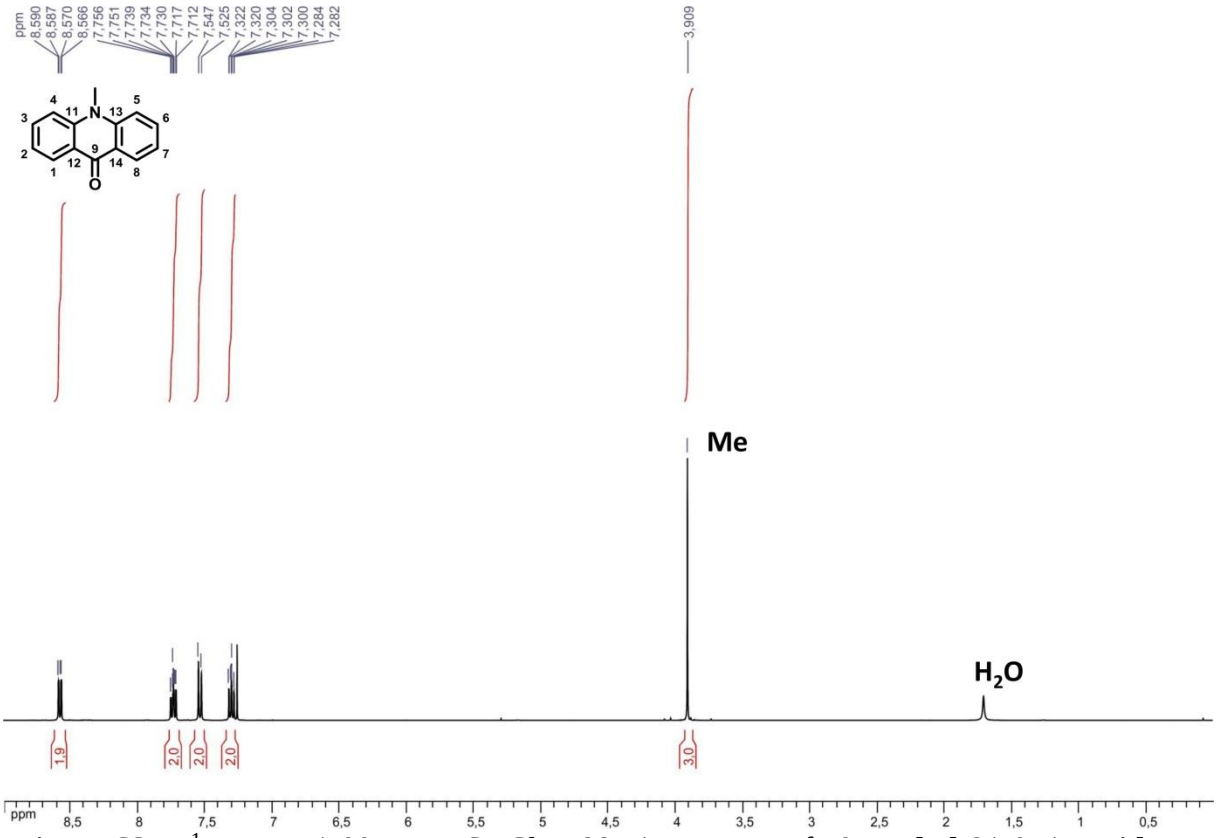

Figure S3.1: ^{1}H NMR (400 MHz, $CDCl_3$, 298 K) spectrum of **10-methyl-9(10H)-acridone**.

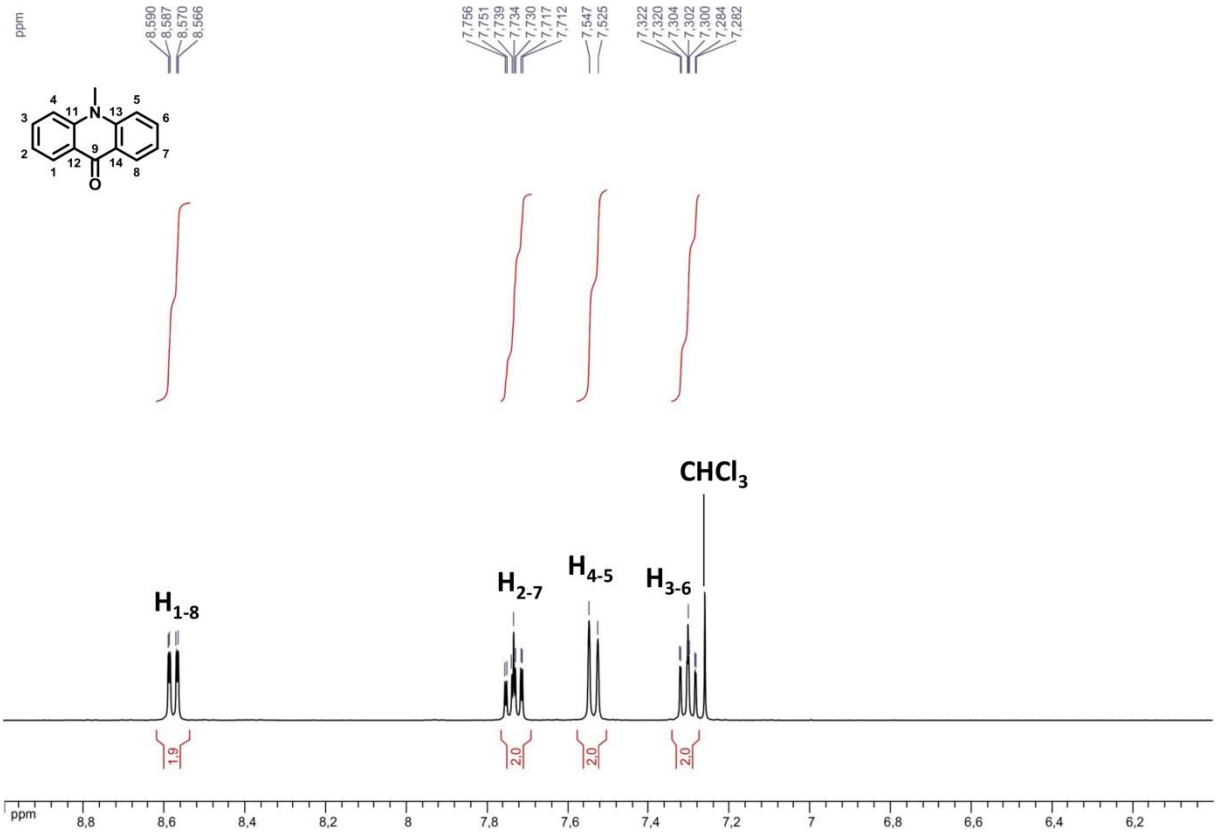

Figure S3.2: ^{1}H NMR (400 MHz, $CDCl_3$, 298 K) spectrum of **10-methyl-9(10H)-acridone** (aromatic region).

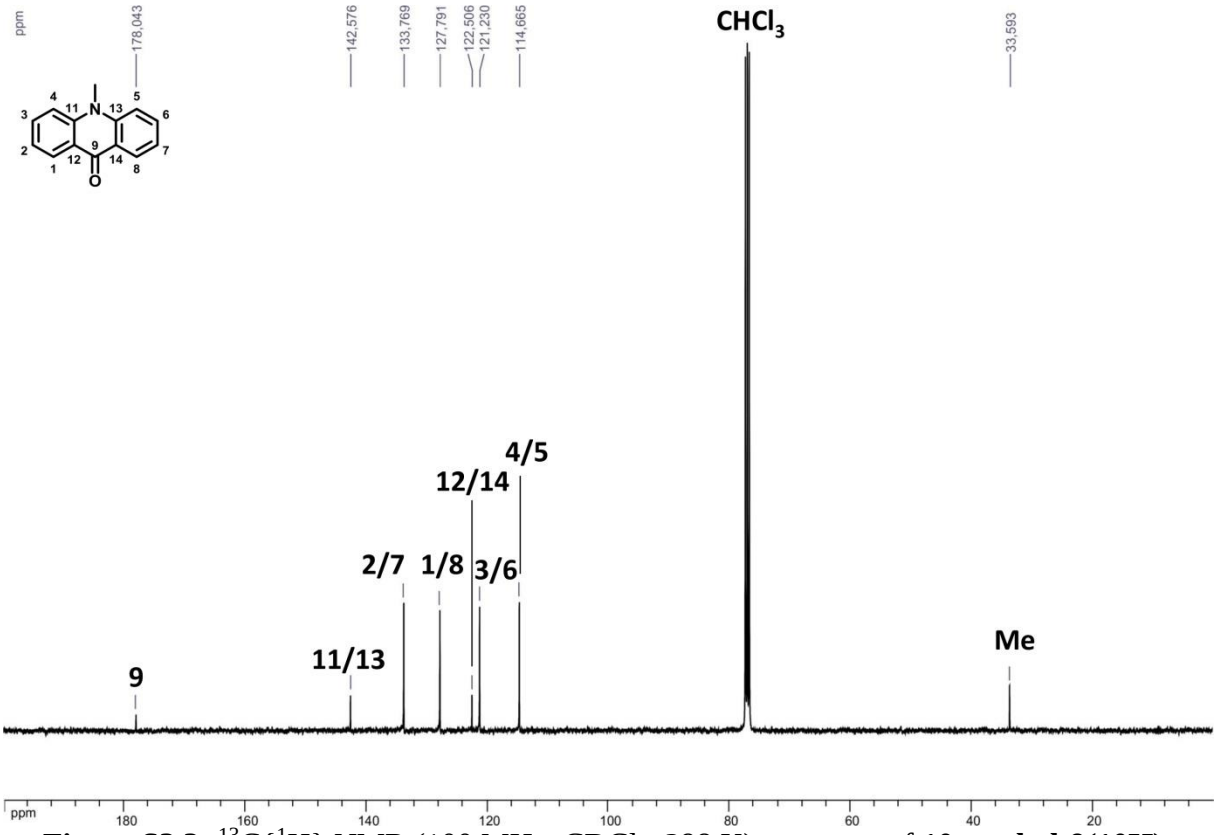

Figure S3.3: $^{13}C\{^{1}H\}$ NMR (100 MHz, $CDCl_3$, 298 K) spectrum of **10-methyl-9(10H)-acridone**.

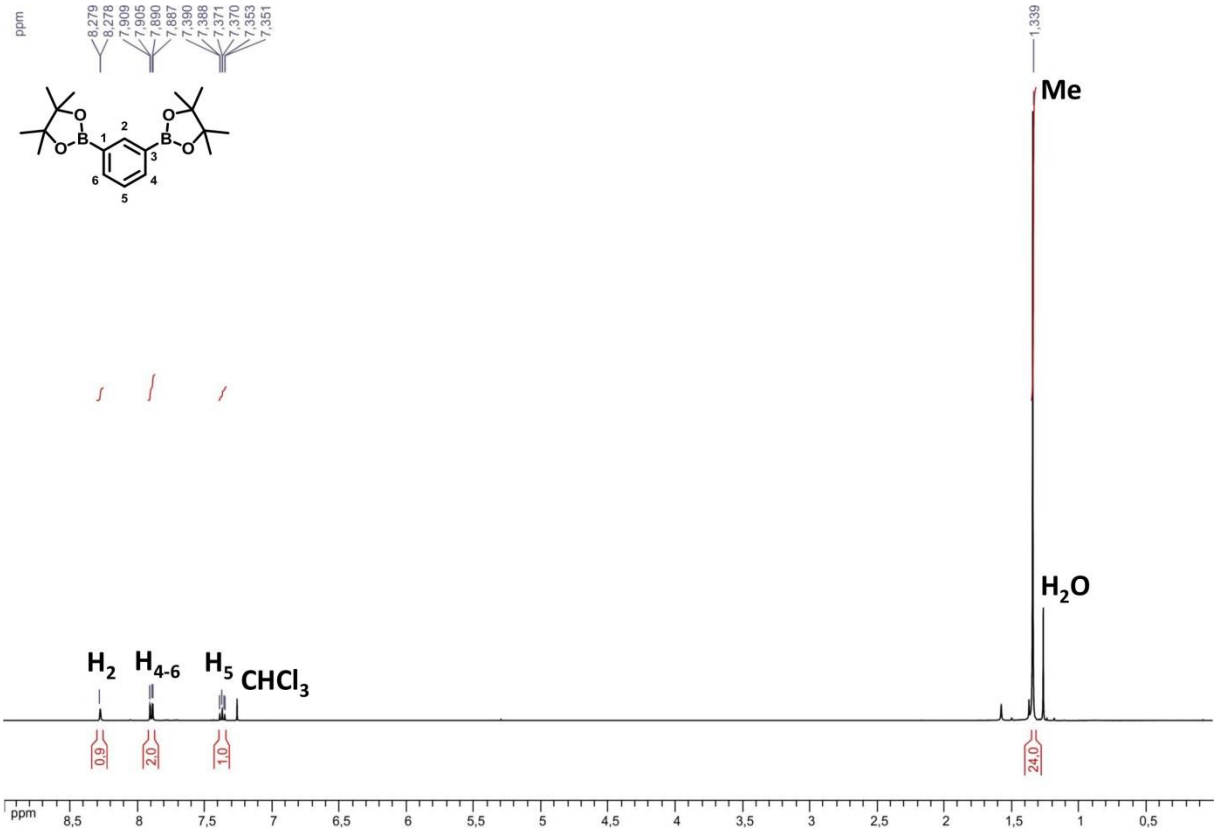

Figure S3.4: ^{1}H NMR (400 MHz, $CDCl_3$, 298 K) spectrum of **2**.

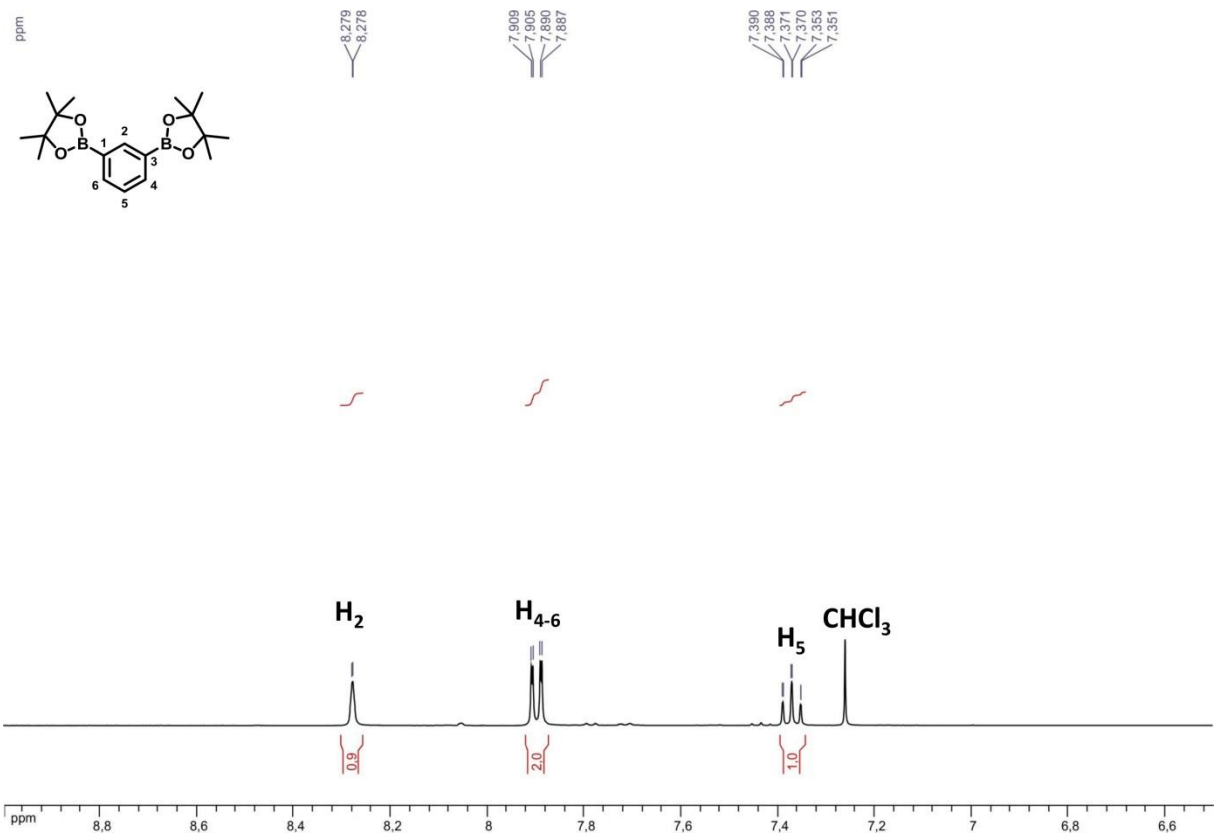

Figure S3.5: ^{1}H NMR (400 MHz, $CDCl_3$, 298 K) spectrum of **2** (aromatic region).

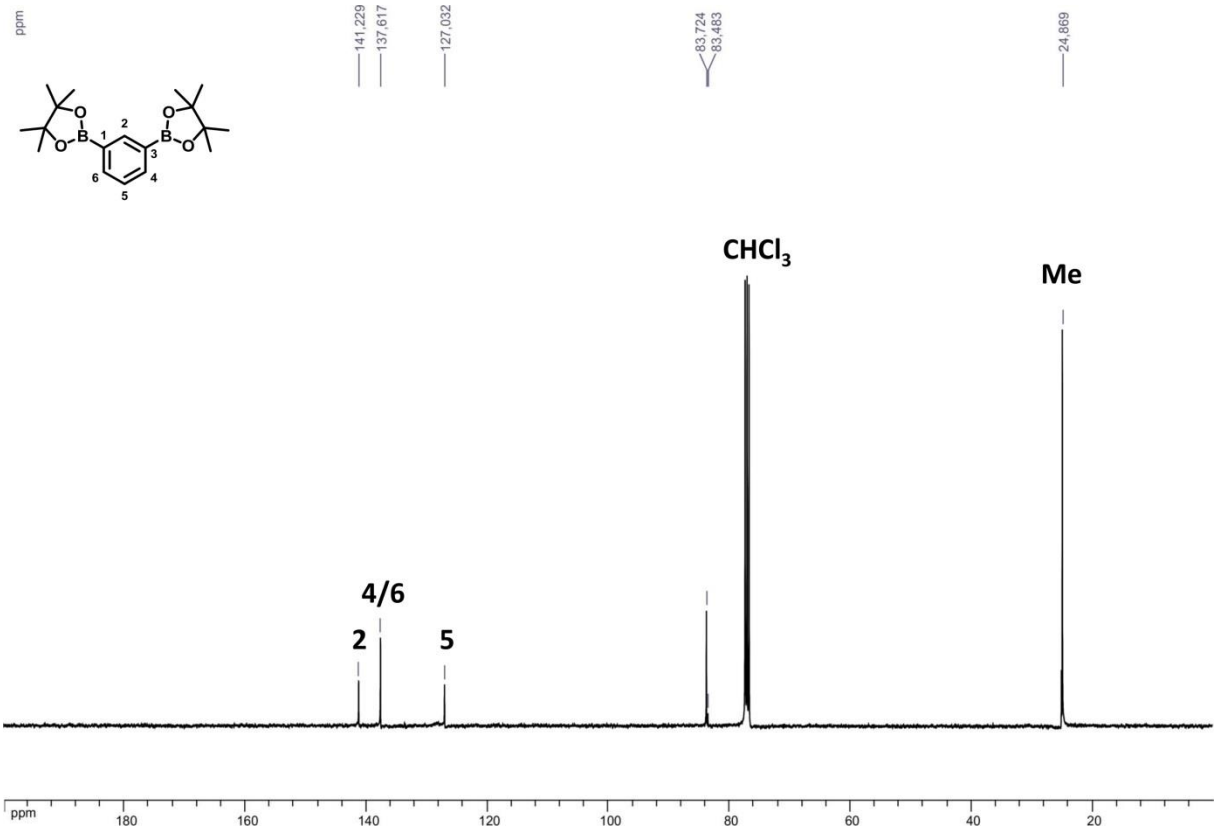

Figure S3.6: ^{13}C{^{1}H} NMR (100 MHz, $CDCl_3$, 298 K) spectrum of **2**.

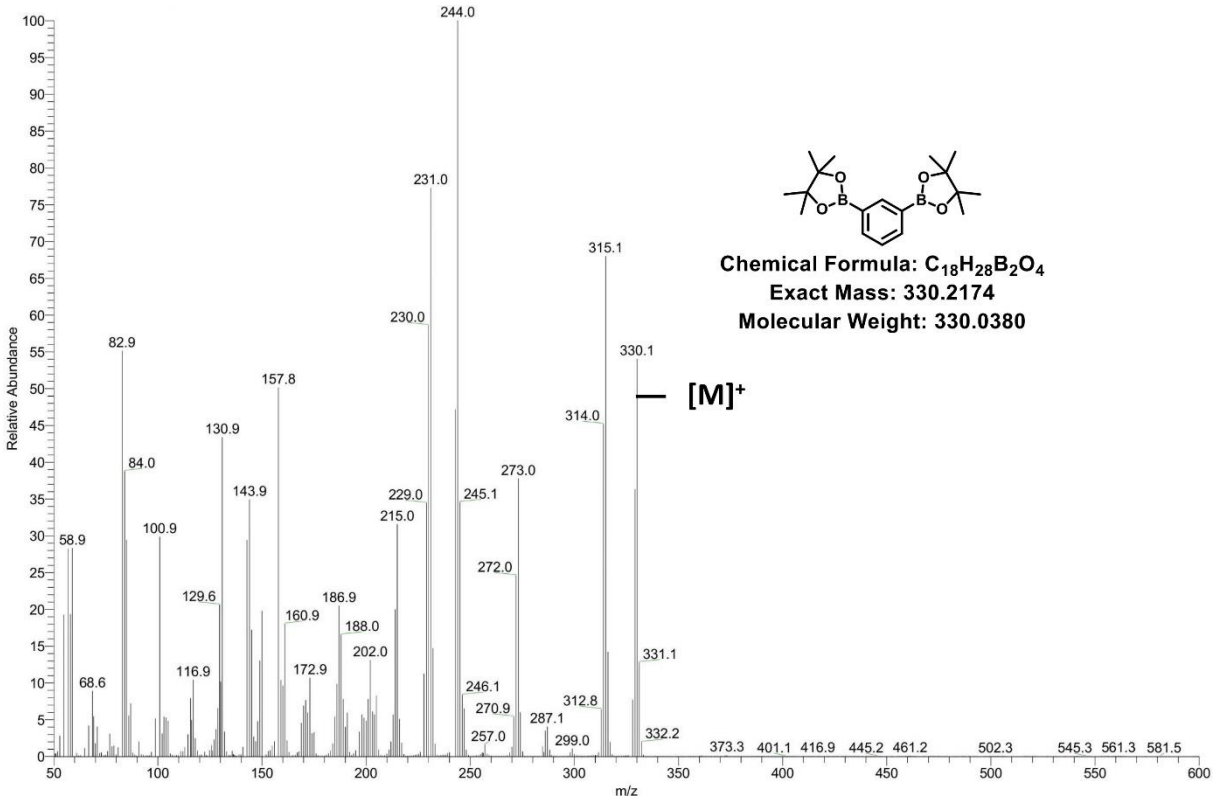

Figure S3.7: Mass Spectrum (EI) of **2**

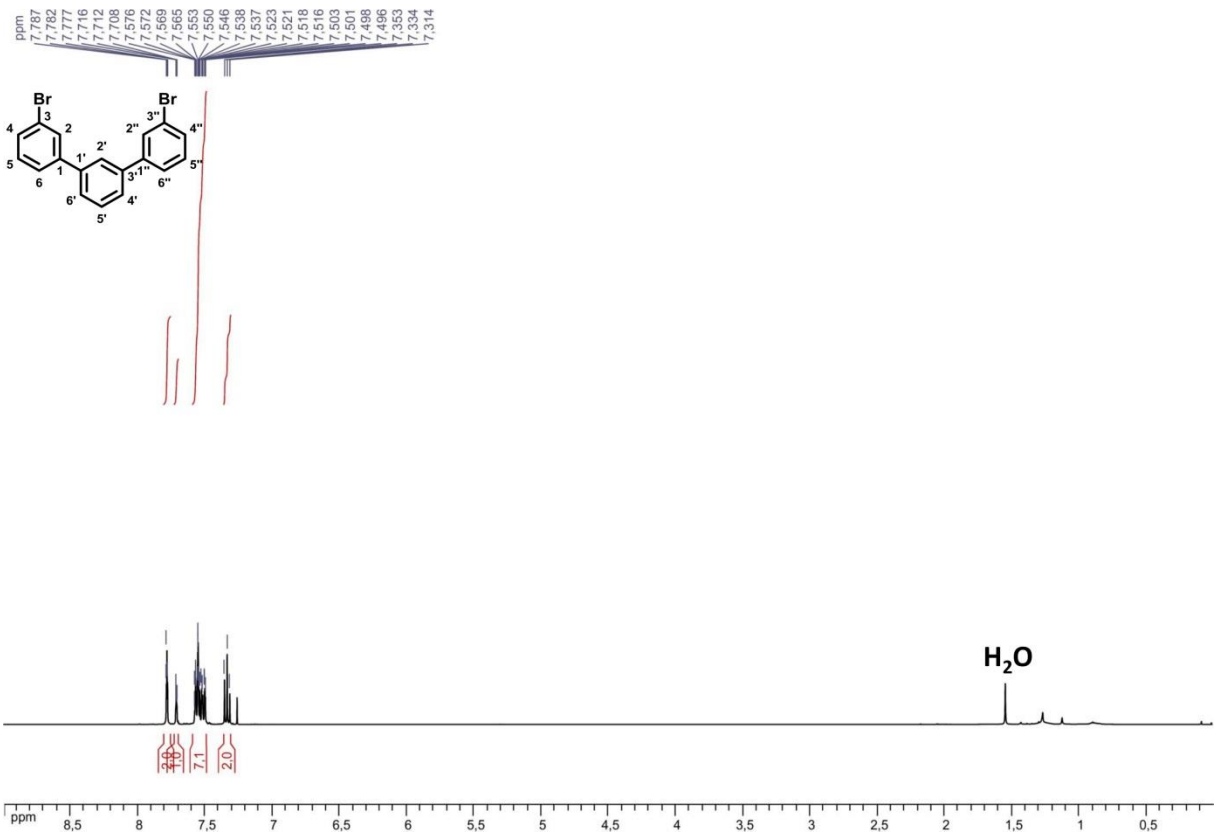

Figure S3.8: ^{1}H NMR (400 MHz, $CDCl_3$, 298 K) spectrum of **3**.

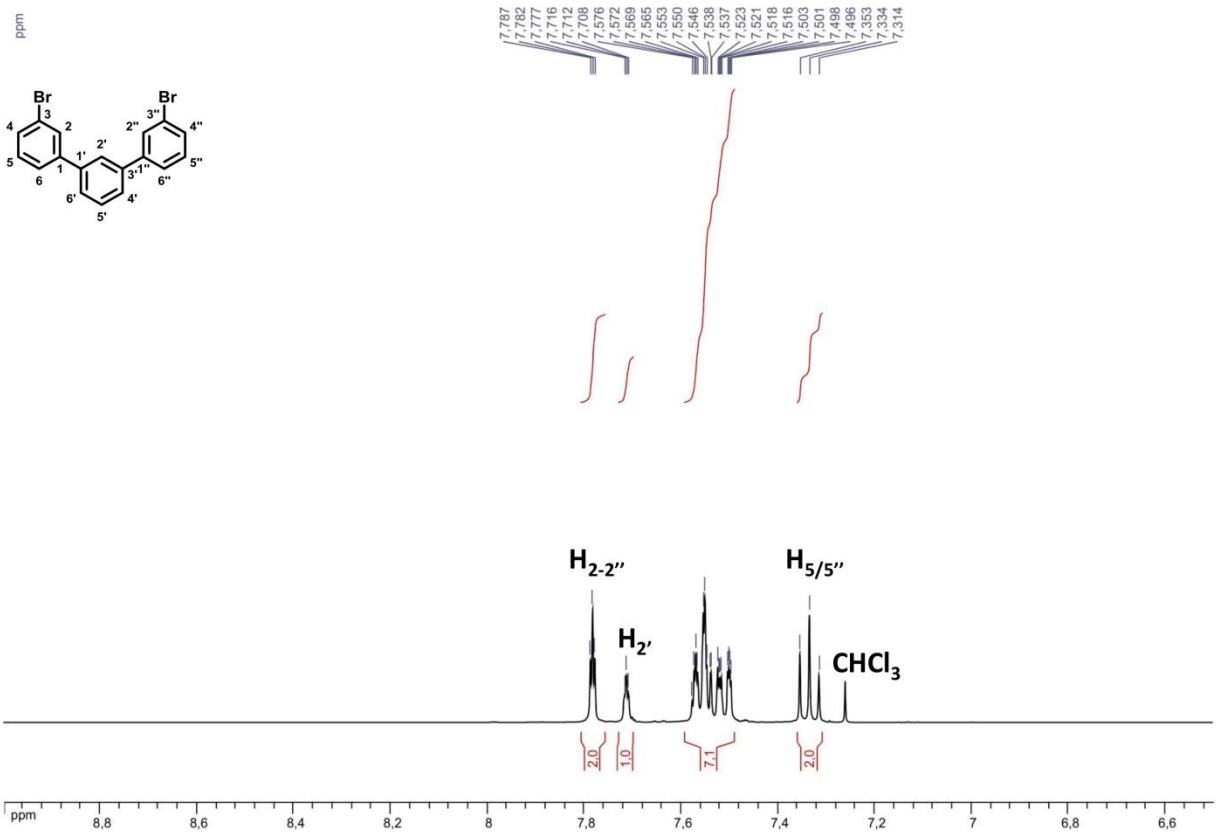

Figure S3.9: ^{1}H NMR (400 MHz, $CDCl_3$, 298 K) spectrum of **3** (aromatic region).

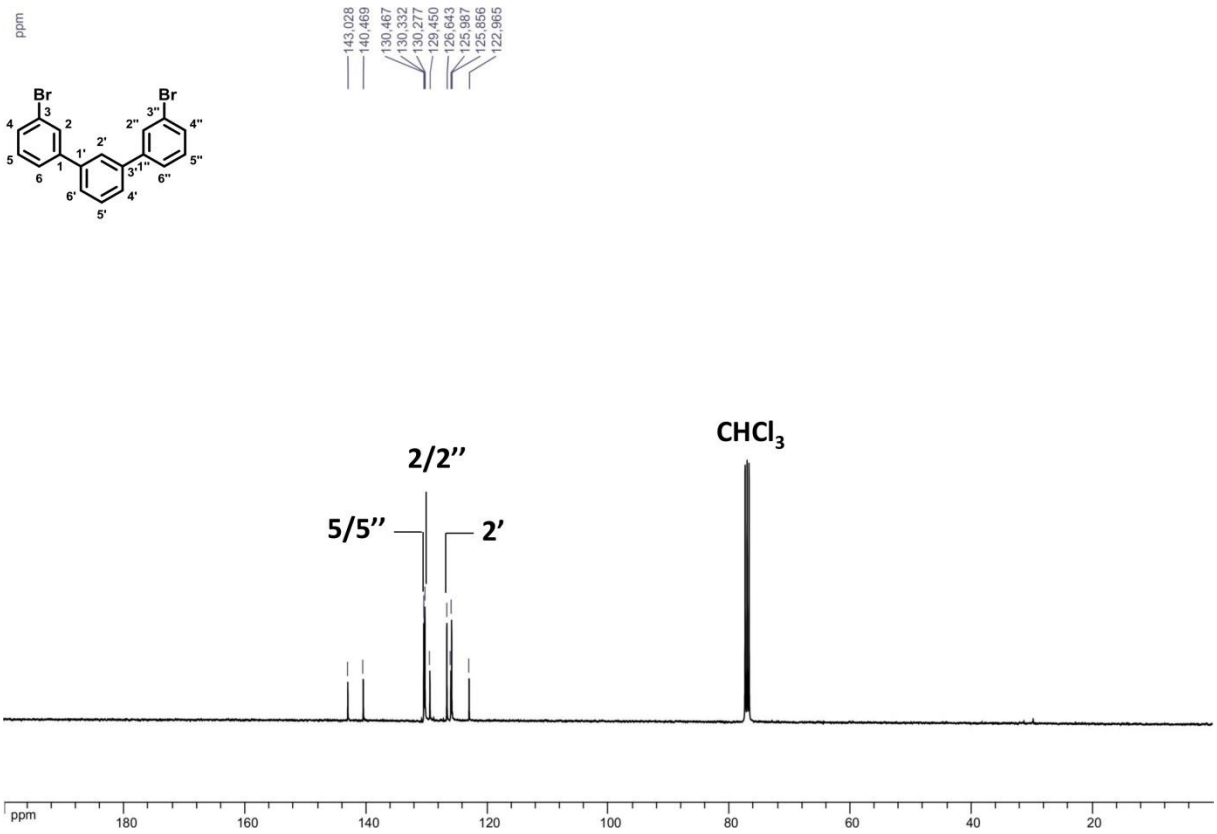

Figure S3.10: ^{13}C{^{1}H} NMR (100 MHz, $CDCl_3$, 298 K) spectrum of **3**.

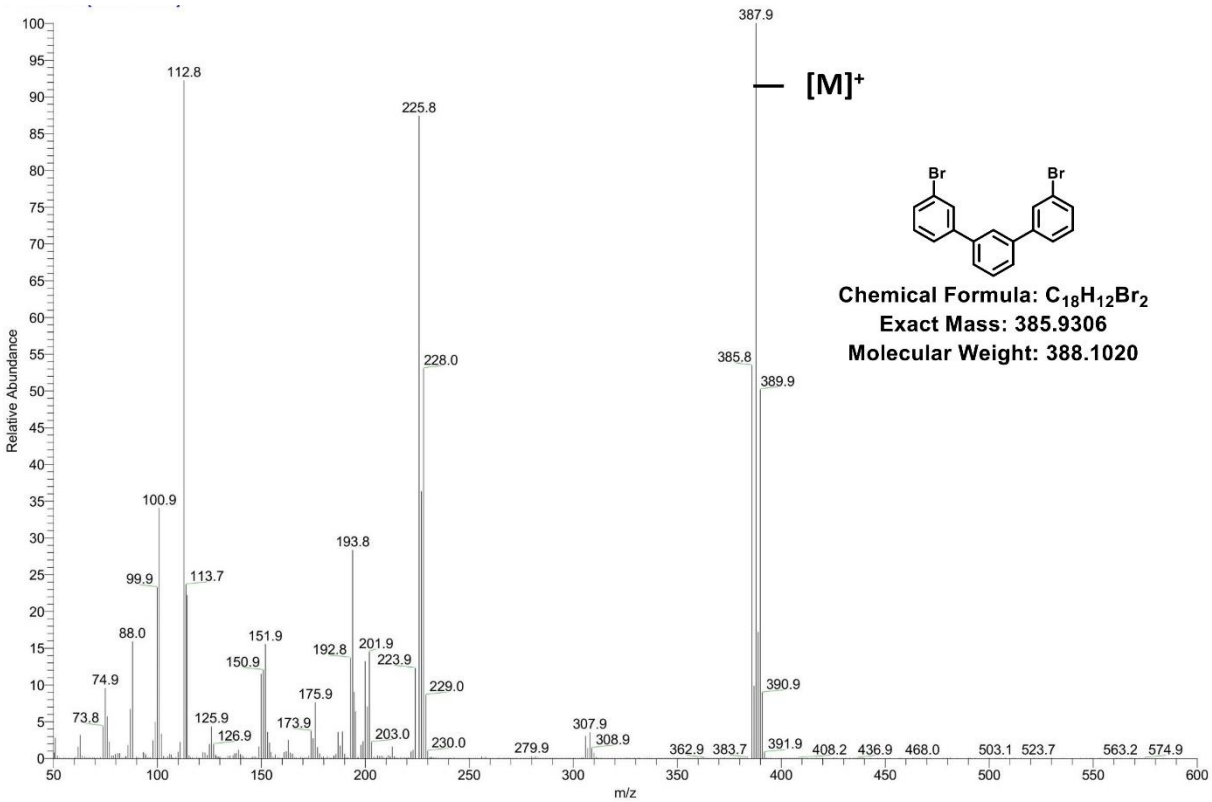

Figure S3.11: Mass Spectrum (EI) of **3**

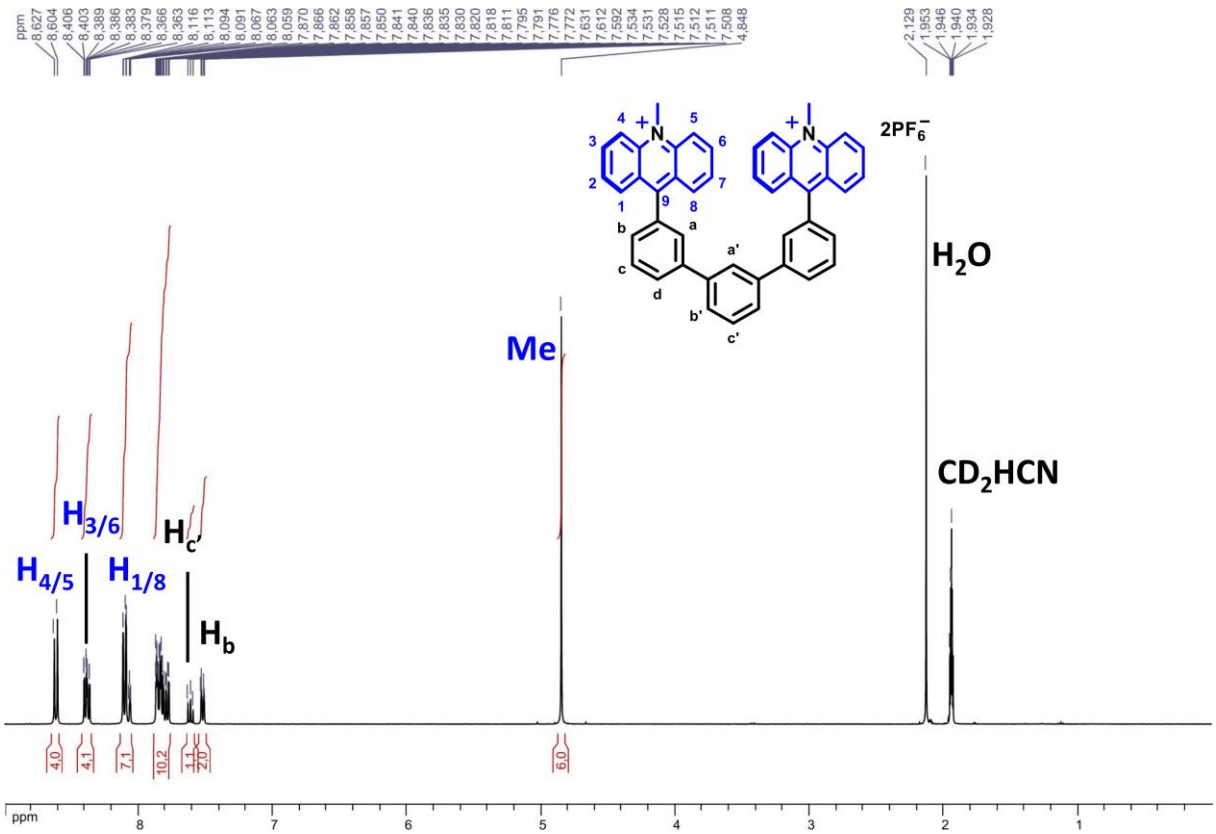

Figure S3.12: ^{1}H NMR (400 MHz, CD_3CN, 298 K) spectrum of **1.2PF6**.

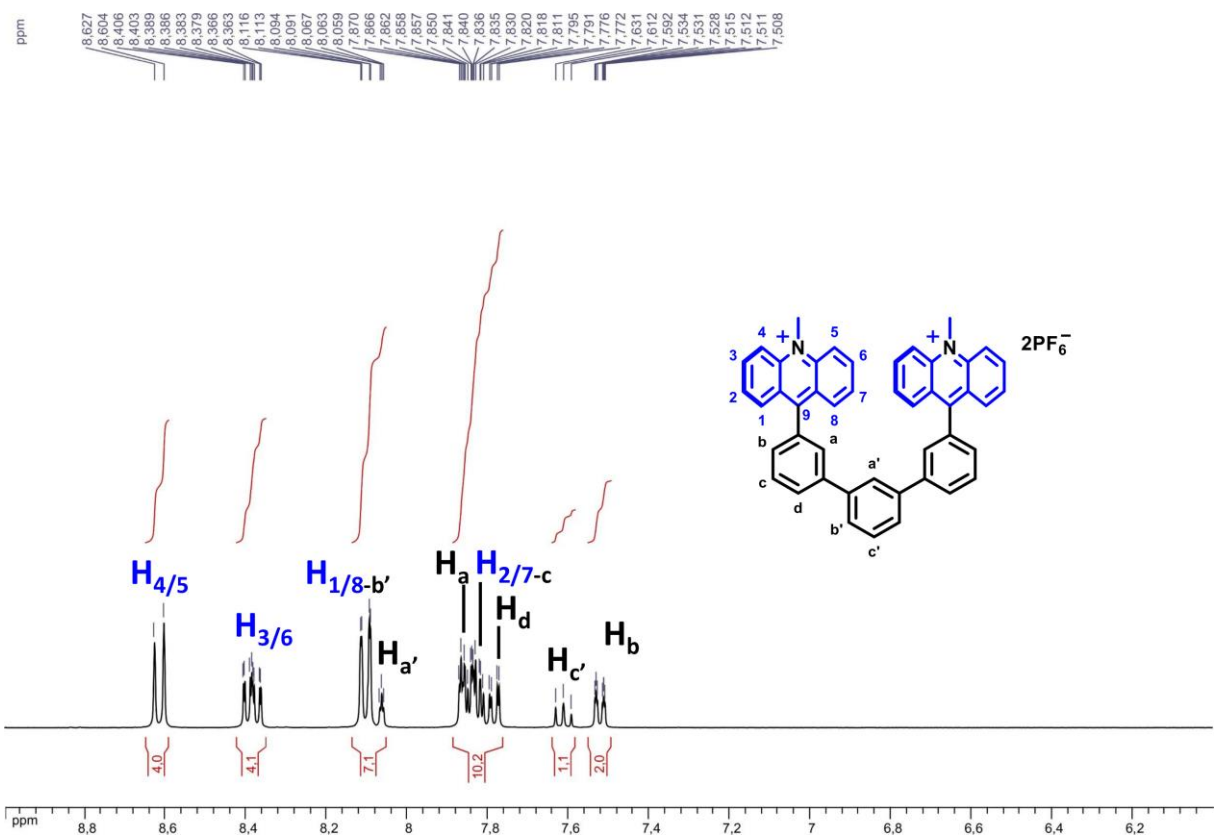

Figure S3.13: ^{1}H NMR (400 MHz, CD_3CN, 298 K) spectrum of **1.2PF$_6$** (aromatic region).

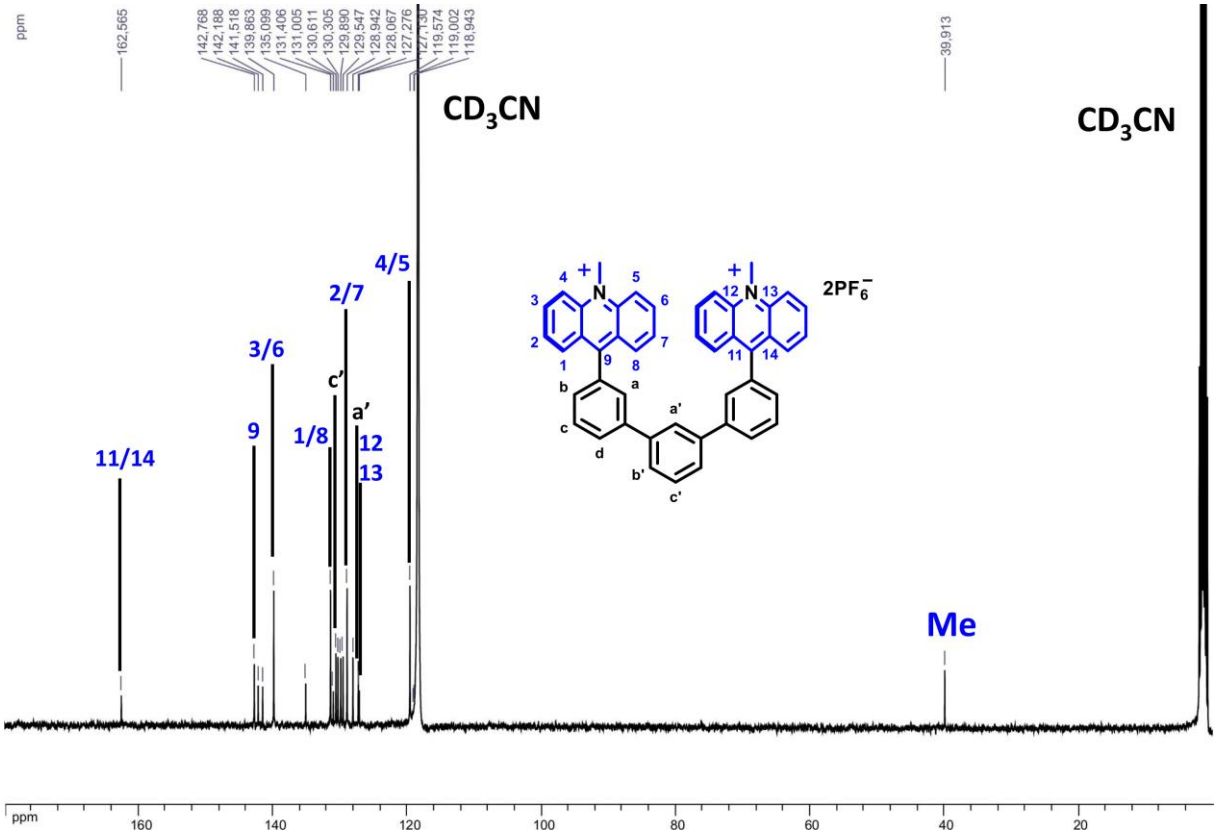

Figure S3.14: ^{13}C{^{1}H} NMR (100 MHz, CD_3CN, 298 K) spectrum of **1.2PF$_6$**.

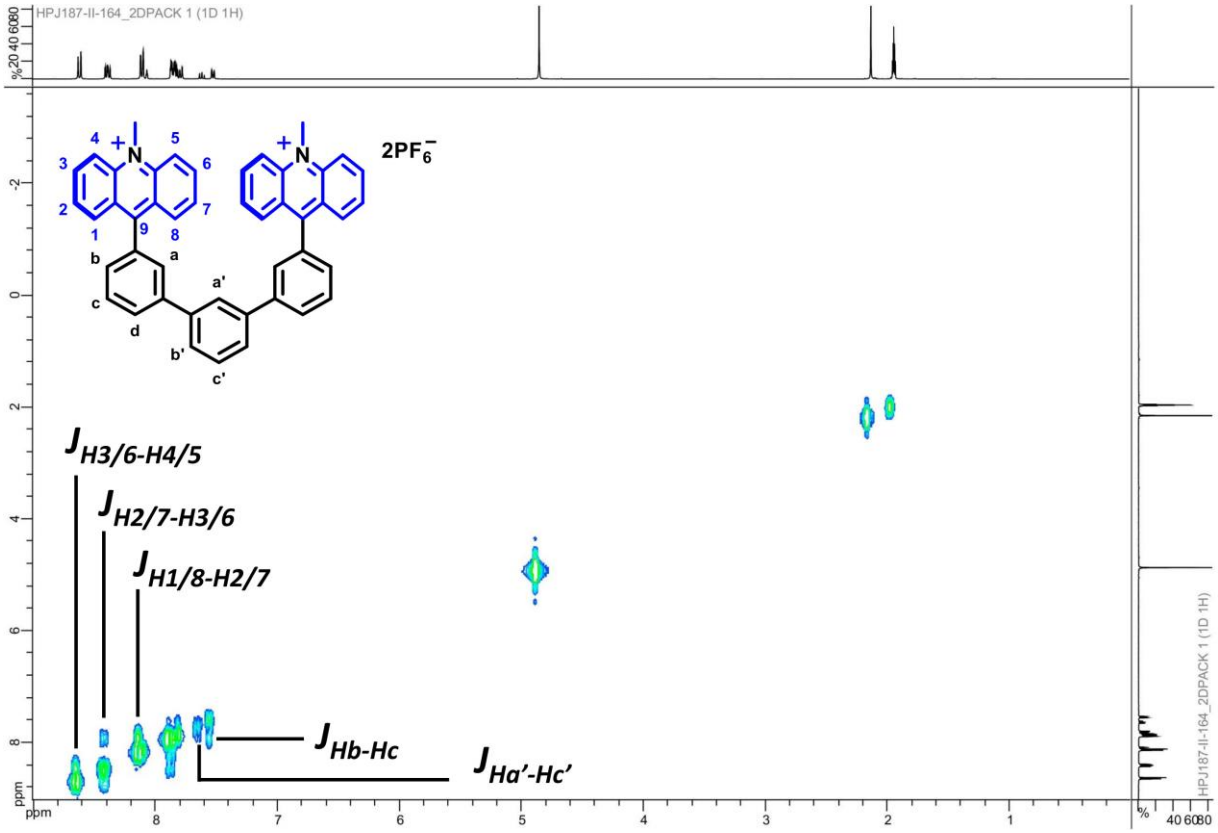

Figure S3.15: ^{1}H–^{1}H gCOSY 2D-spectrum (400 MHz, CD_3CN, 298 K) of **1.2PF$_6$**.

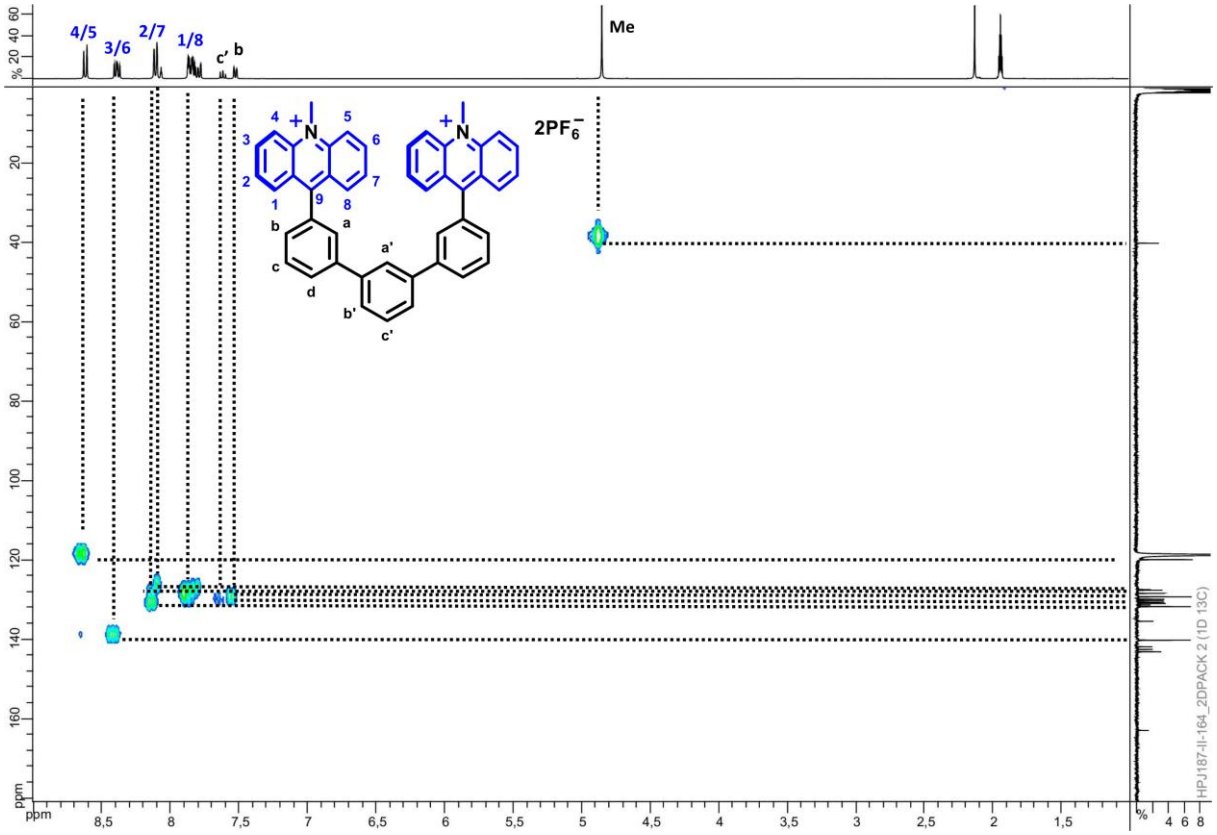

Figure S3.16: ^{1}H–^{13}C gHSQC 2D-spectrum (400 MHz, CD_3CN, 298 K) of **1.2PF$_6$**.

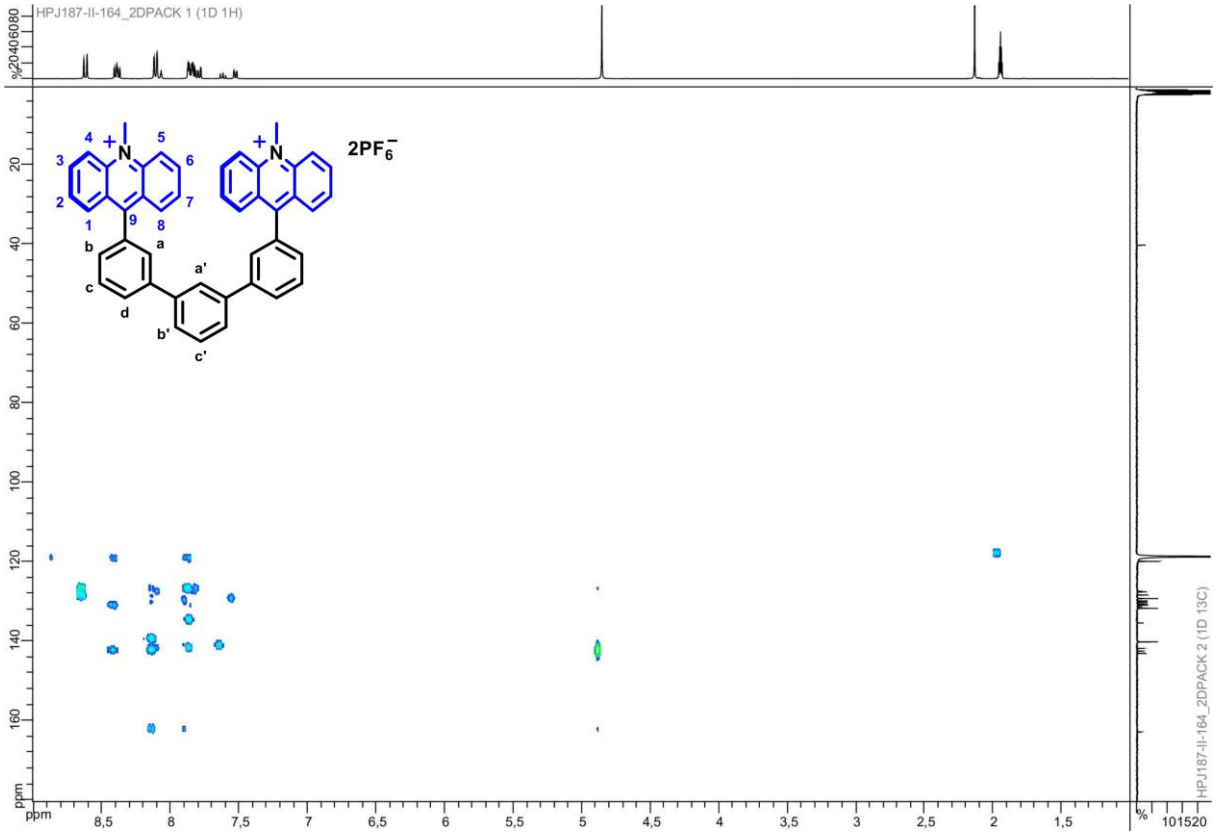

Figure S3.17: $^{1}H–^{13}C$ gHMBC 2D-spectrum (400 MHz, CD_3CN, 298 K) of **1.2PF6**.

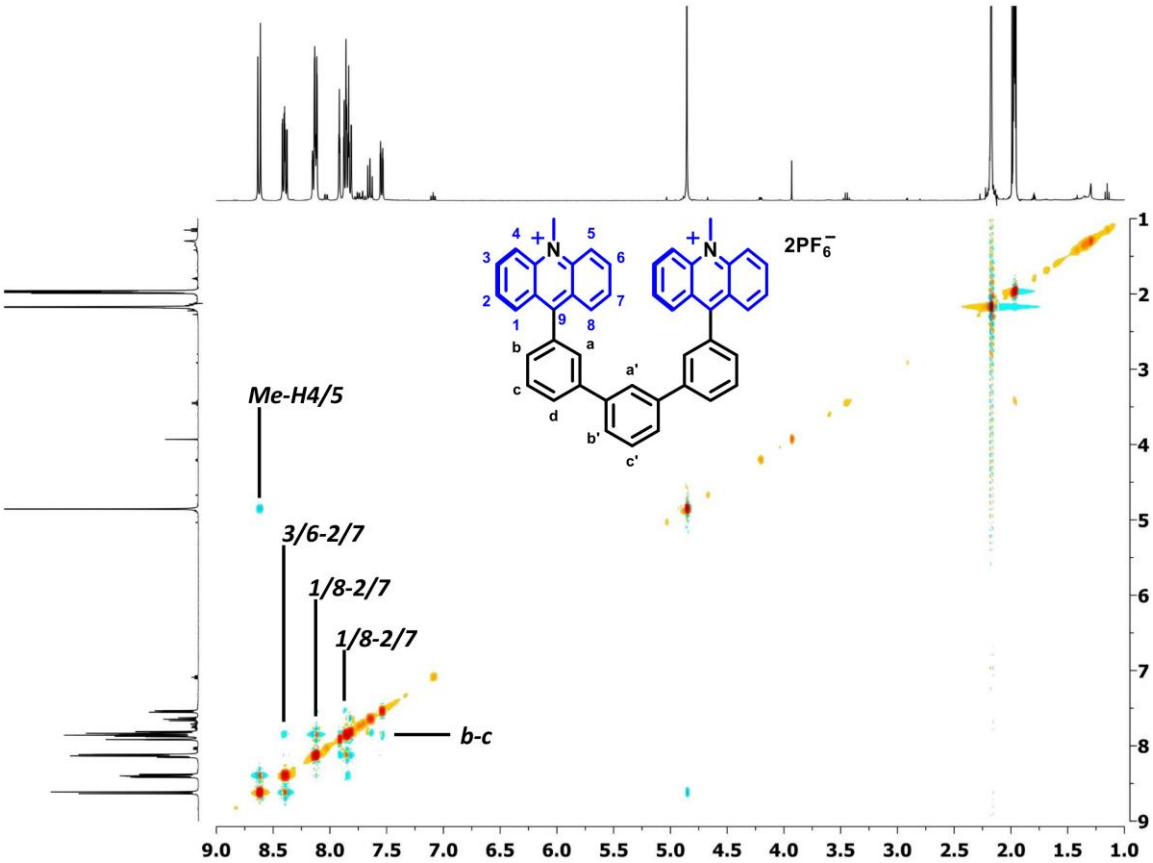

Figure S3.18: $^{1}H–^{1}H$ NOESY 2D-spectrum (400 MHz, CD_3CN, 298 K) of **1.2PF6**.

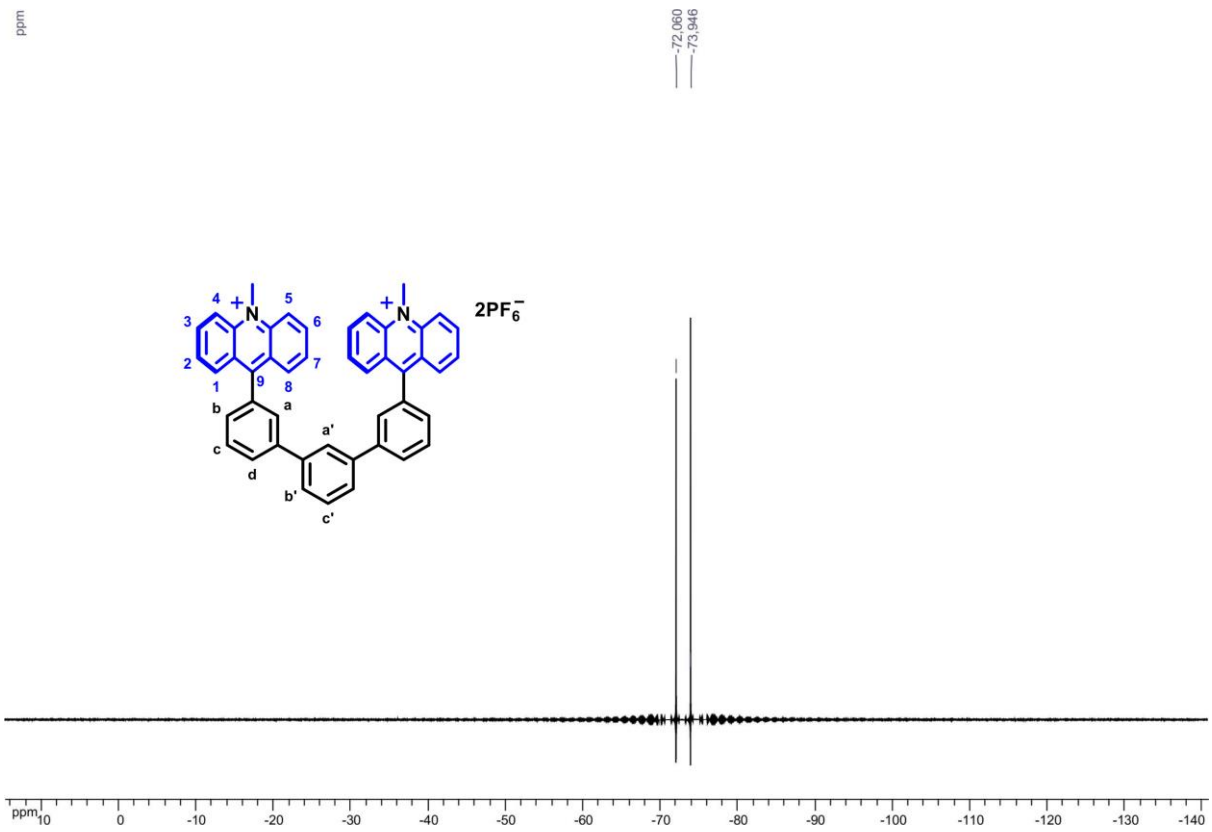

Figure S3.19: $^{19}F\{^{1}H\}$ NMR (376 MHz, CD_3CN, 298 K) spectrum of **1.2PF6**.

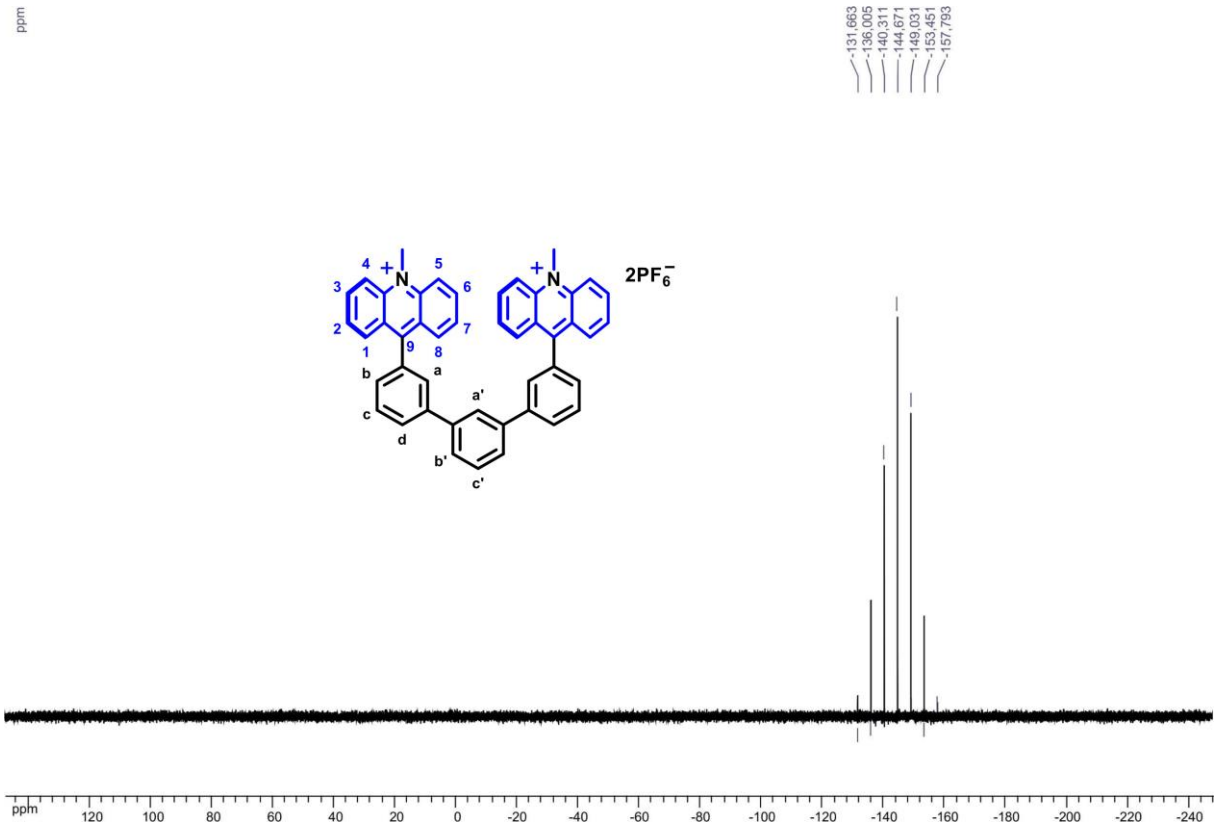

Figure S3.20: $^{31}P\{^{1}H\}$ NMR (162 MHz, CD_3CN, 298 K) spectrum of **1.2PF6**.

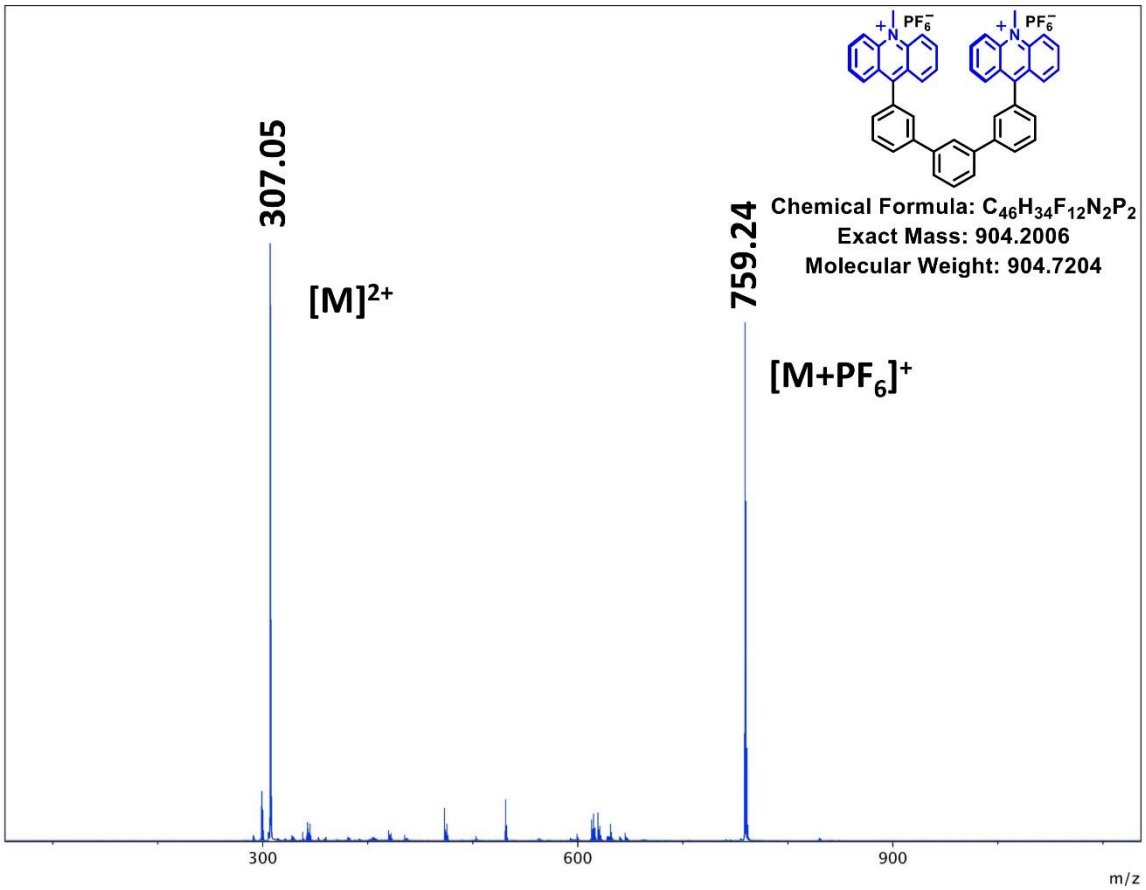

Figure S3.21: Mass Spectrum (ESI) of **1.2PF$_6$**.

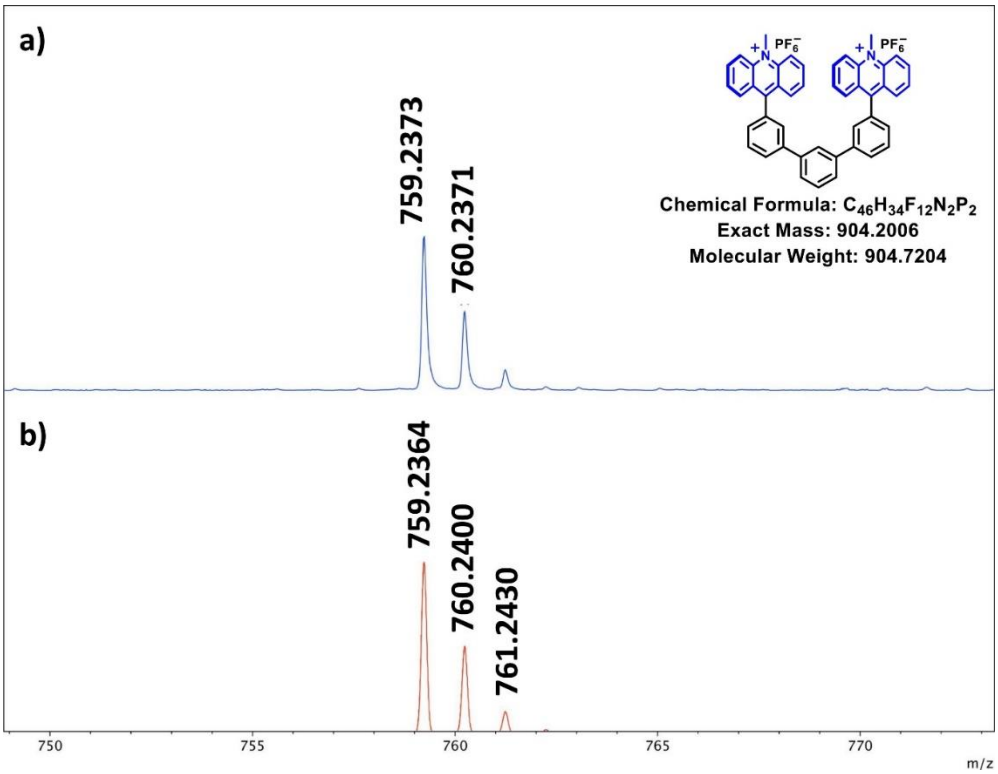

Figure S3.22: Zoom on the $[M–PF_6]^+$ isotopic pattern of the Mass Spectrum (ESI) of **1.2PF$_6$**. a) Low Resolution. b) High Resolution.

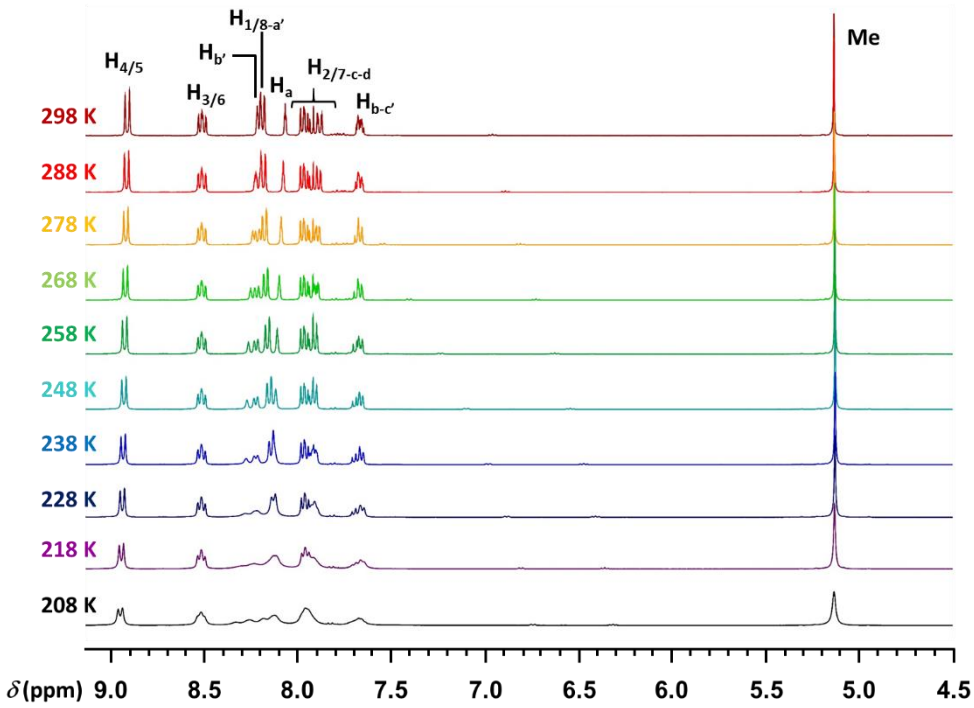

Figure S3.23: ^{1}H NMR (400 MHz, acetone-d^6) spectrum of **1.2PF$_6$** from 298 K to 208 K.

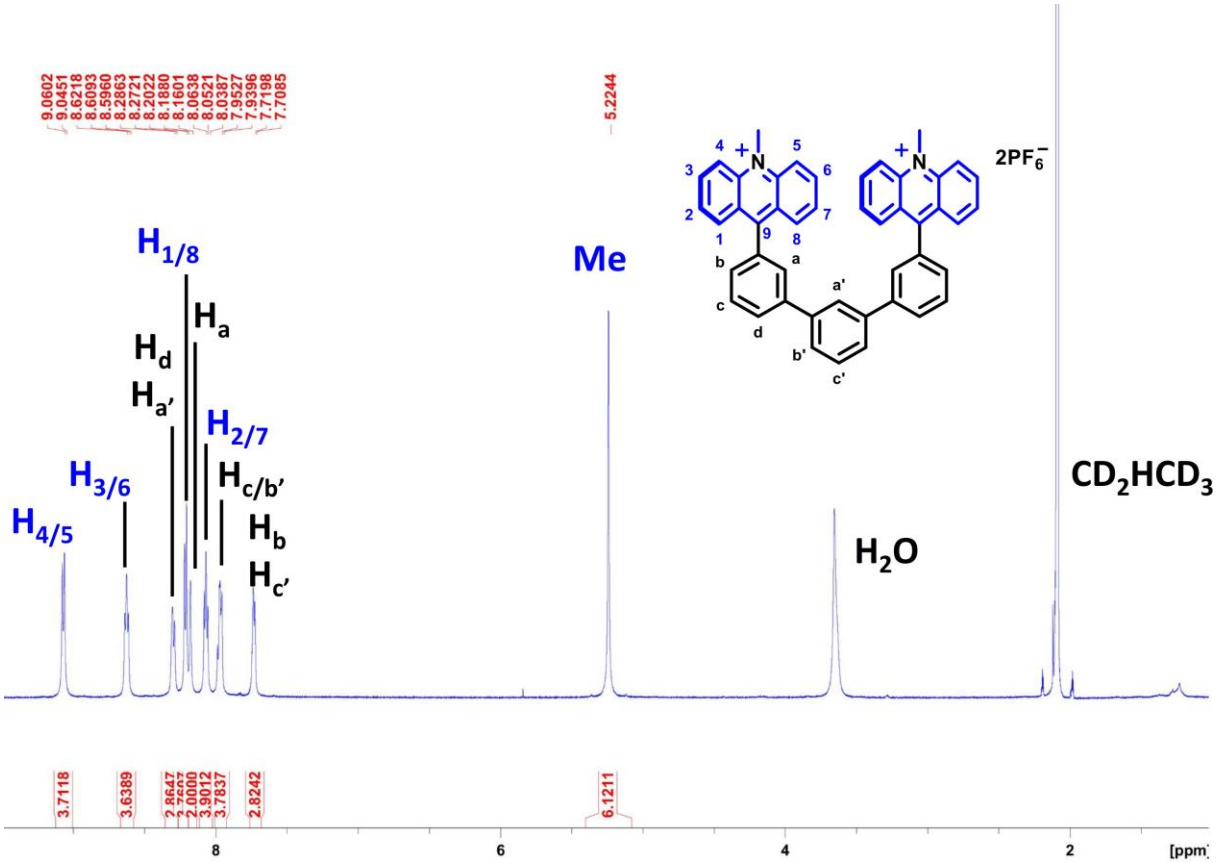

Figure S3.24: ^{1}H NMR (600 MHz, Acetone-d^6, 193 K) spectrum of **1.2PF$_6$**.

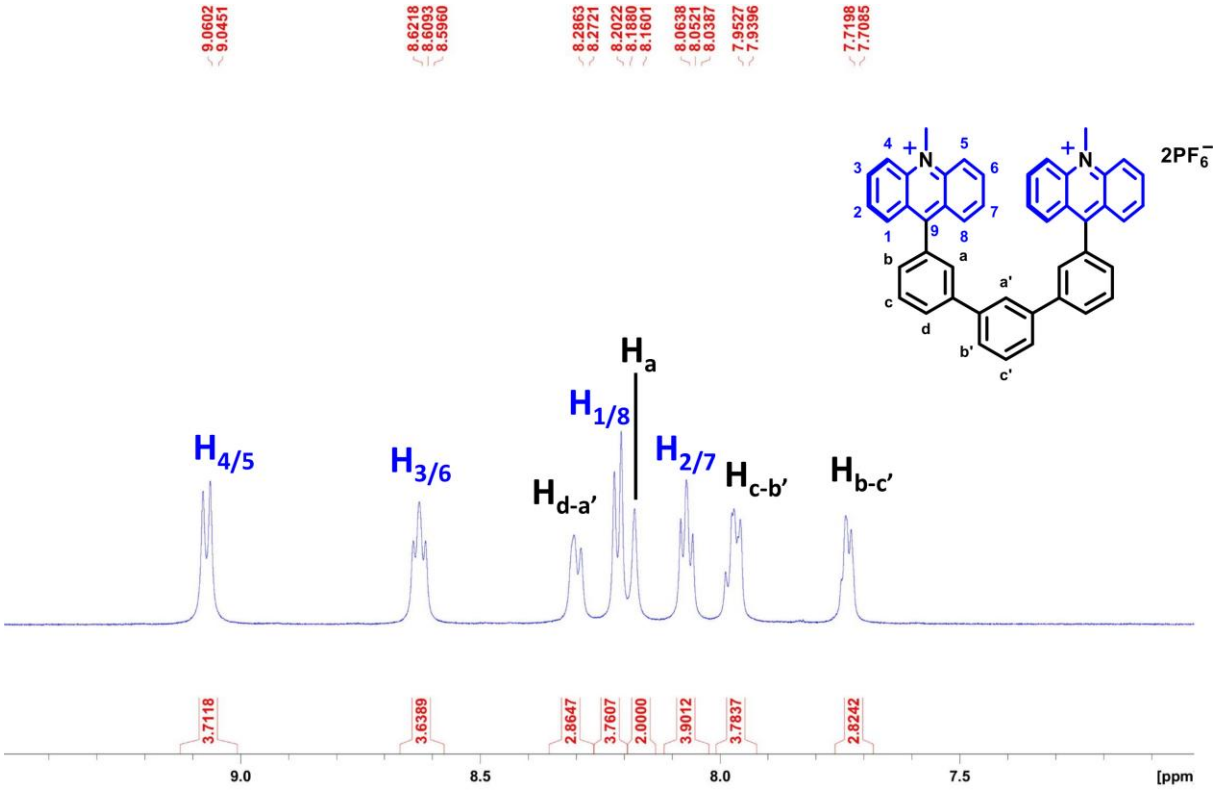

Figure S3.25: ^{1}H NMR (600 MHz, Acetone-d^6, 193 K) spectrum of **1.2PF$_6$** (aromatic region).

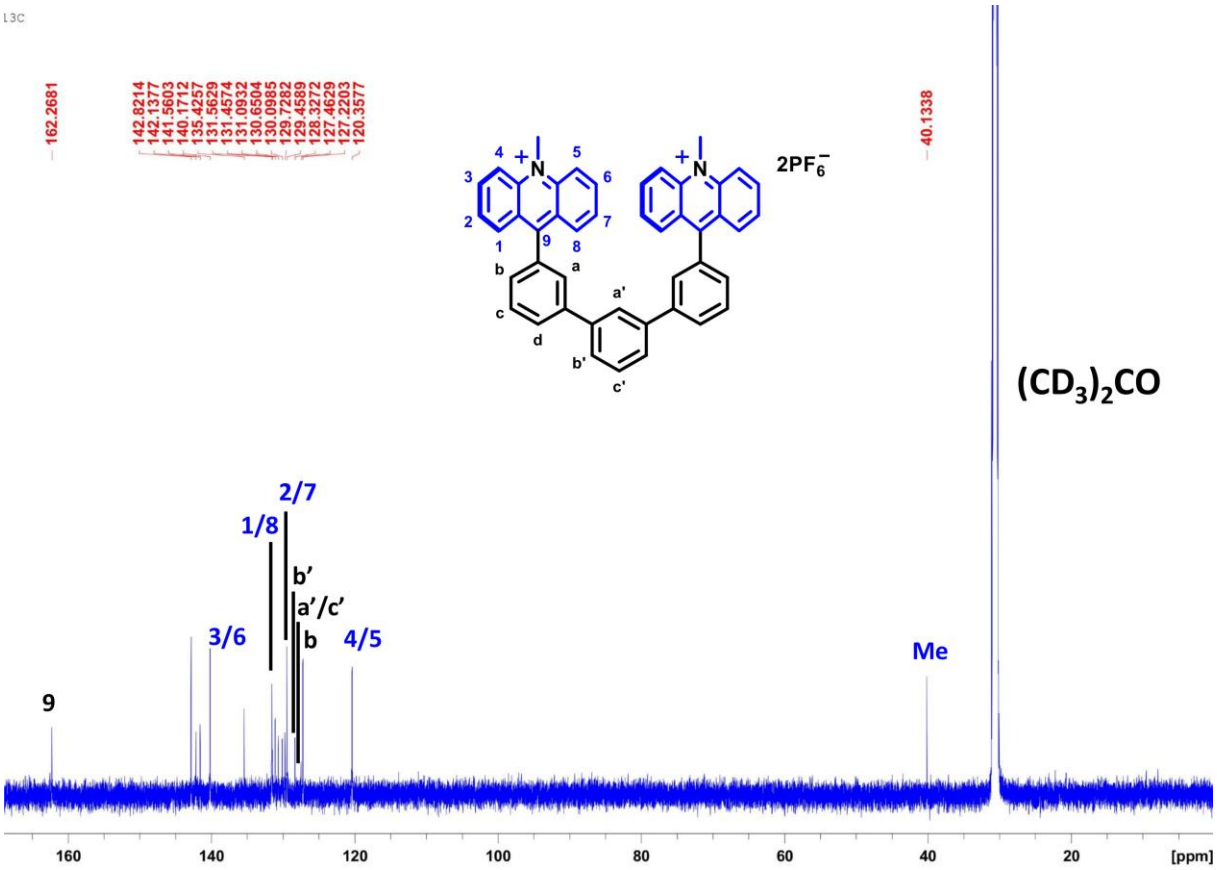

Figure S3.26: ^{13}C{^{1}H} NMR (150 MHz, Acetone-d^6, 193 K) spectrum of **1.2PF$_6$**.

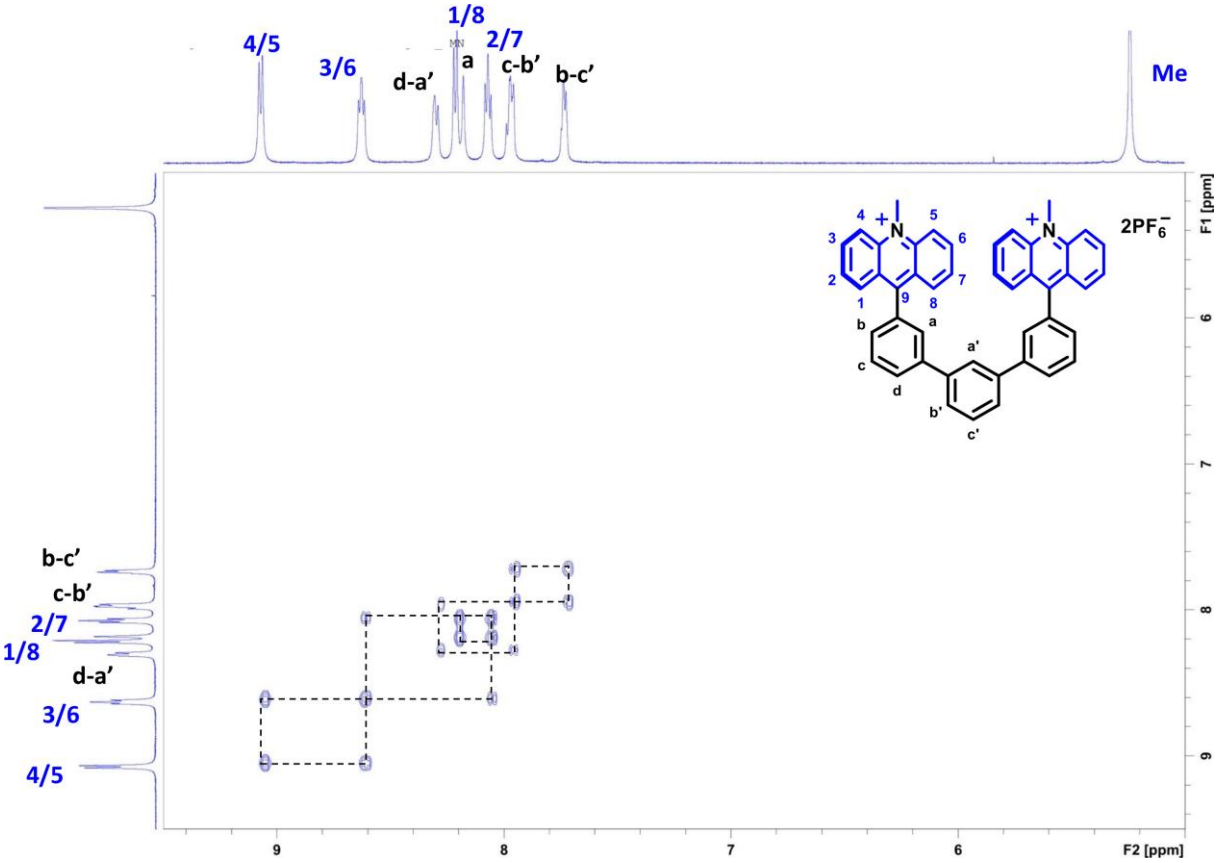

Figure S3.27: ^{1}H–^{1}H gCOSY 2D-spectrum (600 MHz, Acetone-*d*^{6}, 193 K) of **1.2PF$_6$.**

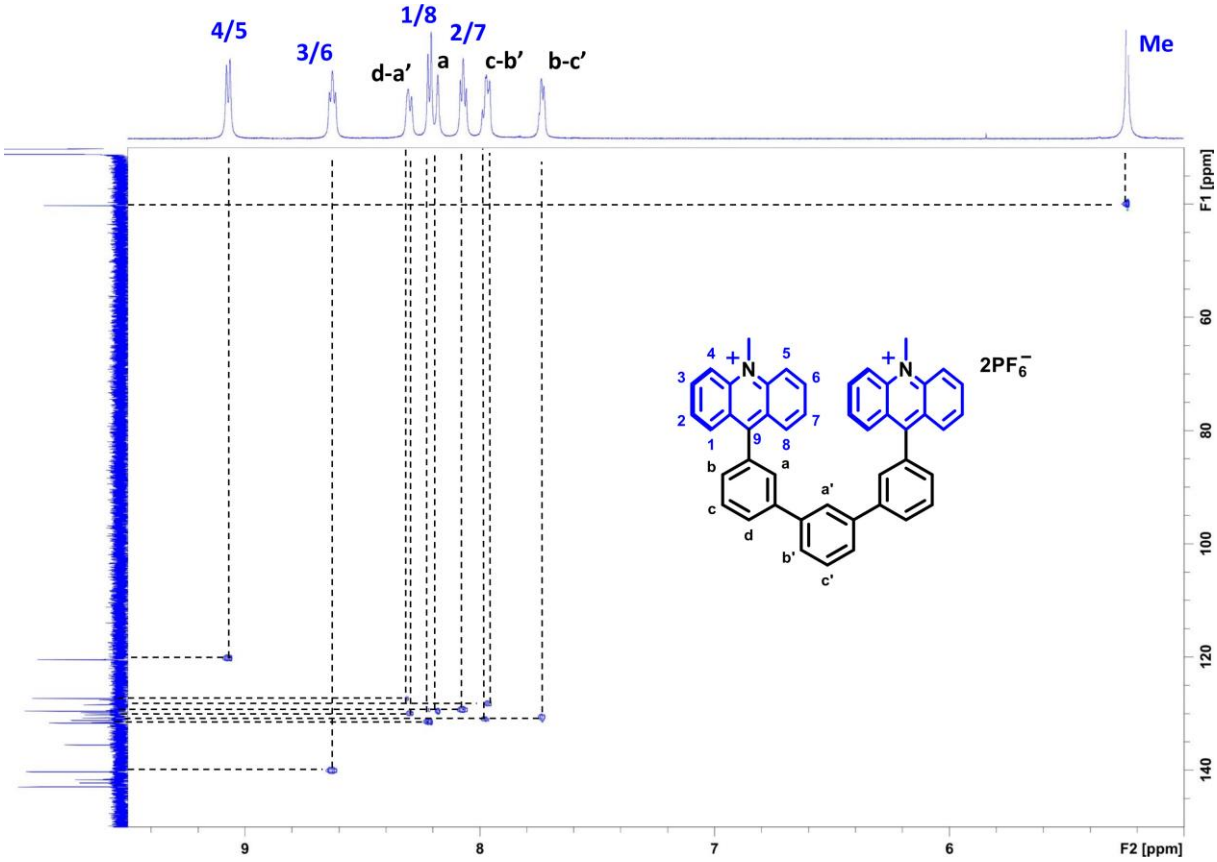

Figure S3.28: ^{1}H–^{13}C gHSQC 2D-spectrum (600 MHz, Acetone-*d*^{6}, 193 K) of **1.2PF$_6$.**

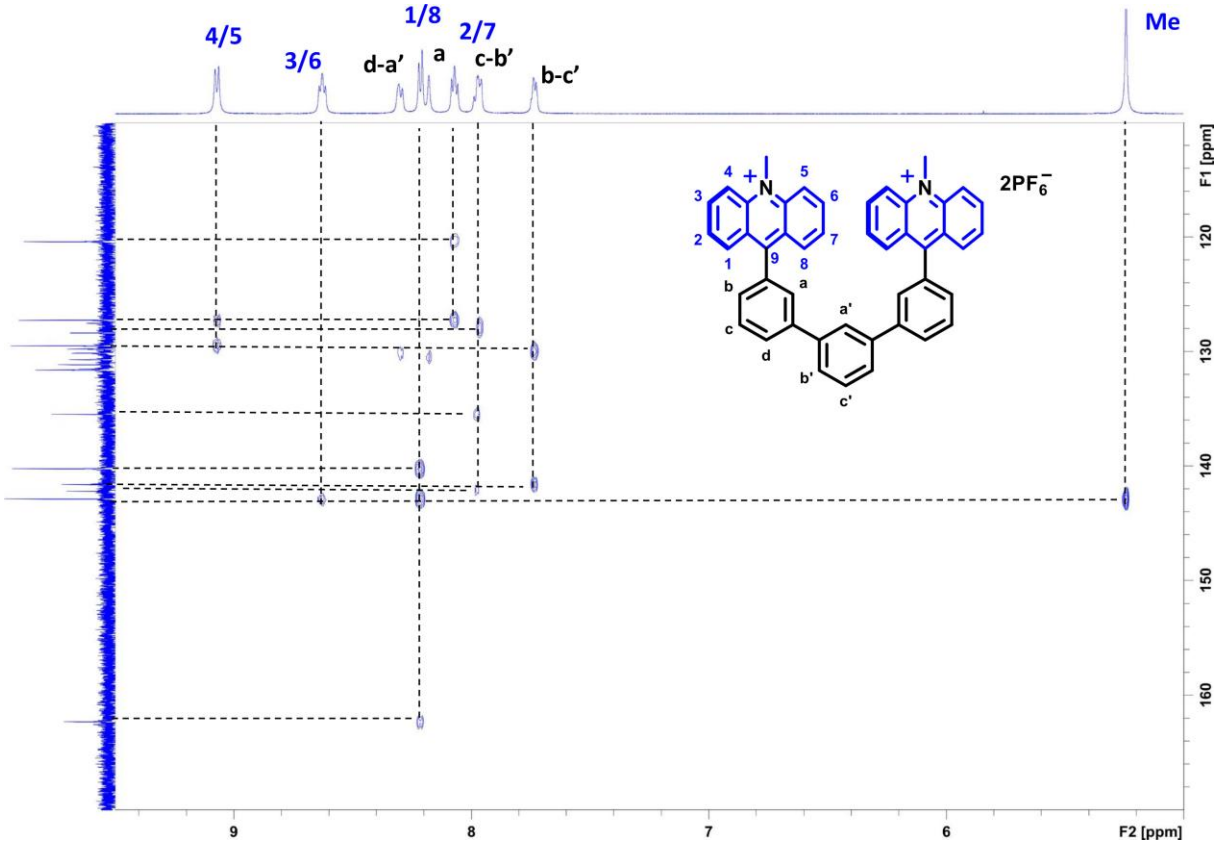

Figure S3.29: ^{1}H–^{13}C gHMBC 2D-spectrum (600 MHz, Acetone-*d*^{6}, 193 K) of **1.2PF$_6$.**

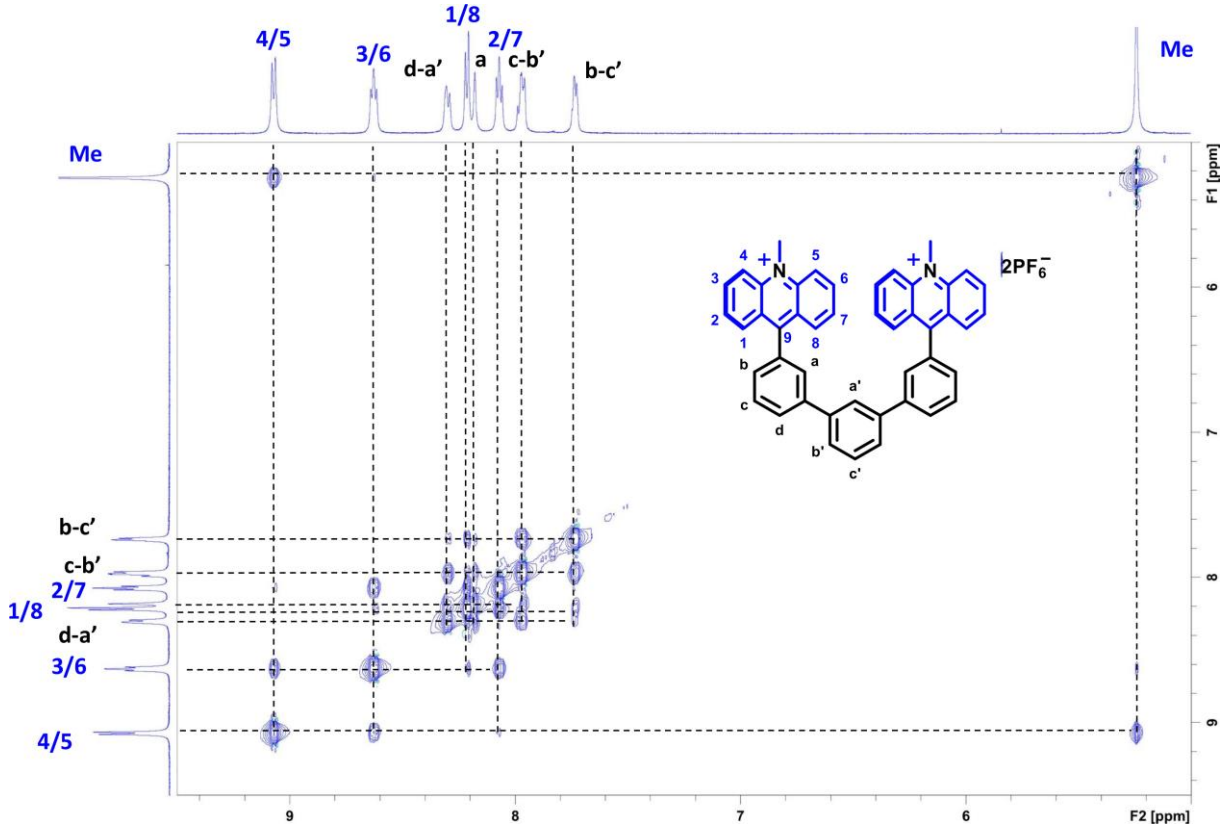

Figure S3.30: ^{1}H–^{1}H NOESY 2D-spectrum (600 MHz, Acetone-*d*^{6}, 193 K) of **1.2PF$_6$**

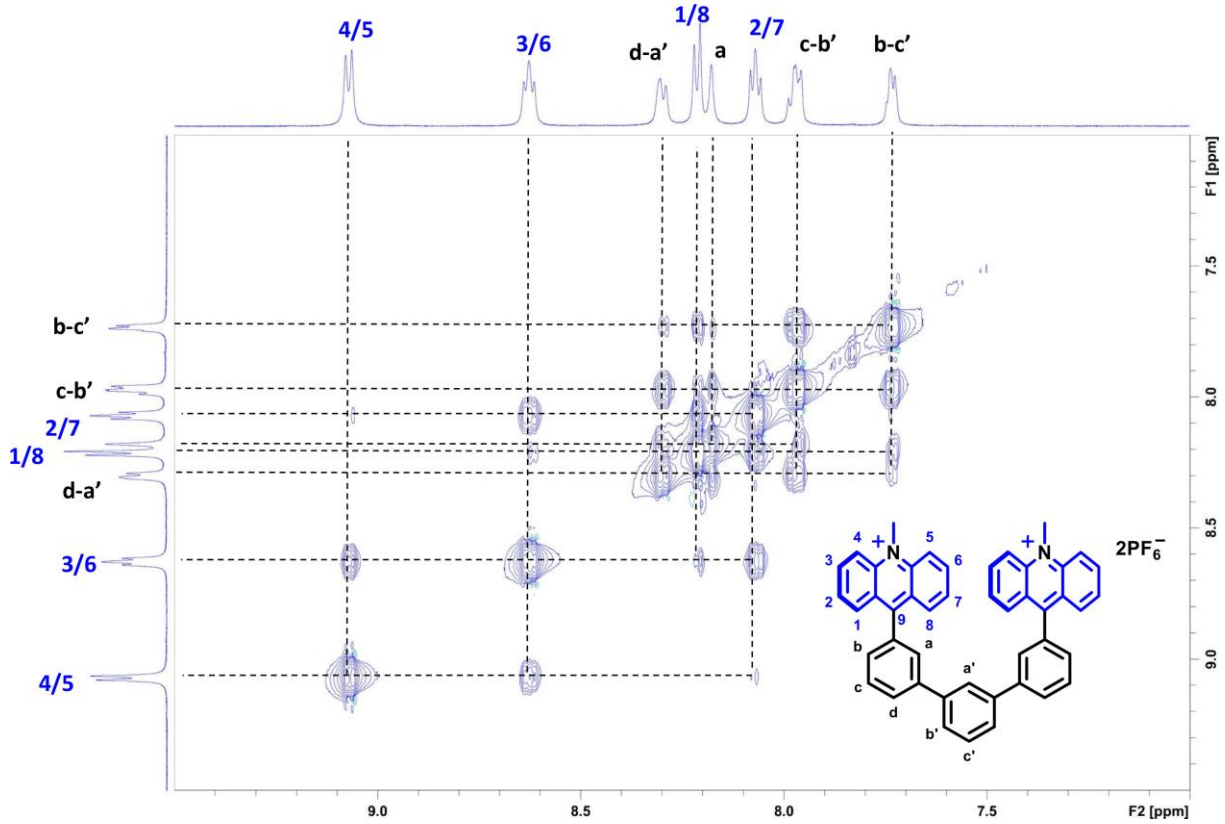

Figure S3.31: ^{1}H–^{1}H NOESY 2D-spectrum (600 MHz, Acetone-d^6, 193 K) of **1.2PF$_6$** (aromatic region).

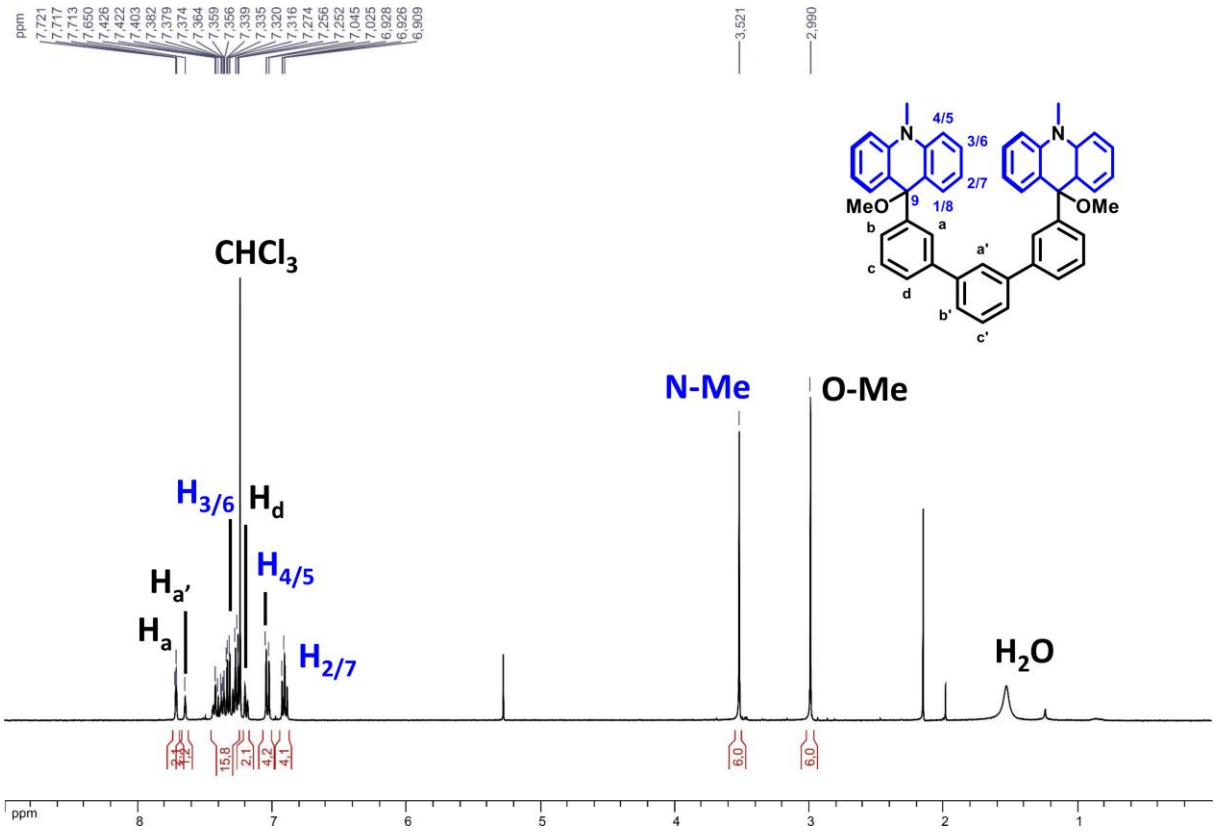

Figure S3.32: ^{1}H NMR (400 MHz, $CDCl_3$, 298 K) spectrum of **4**.

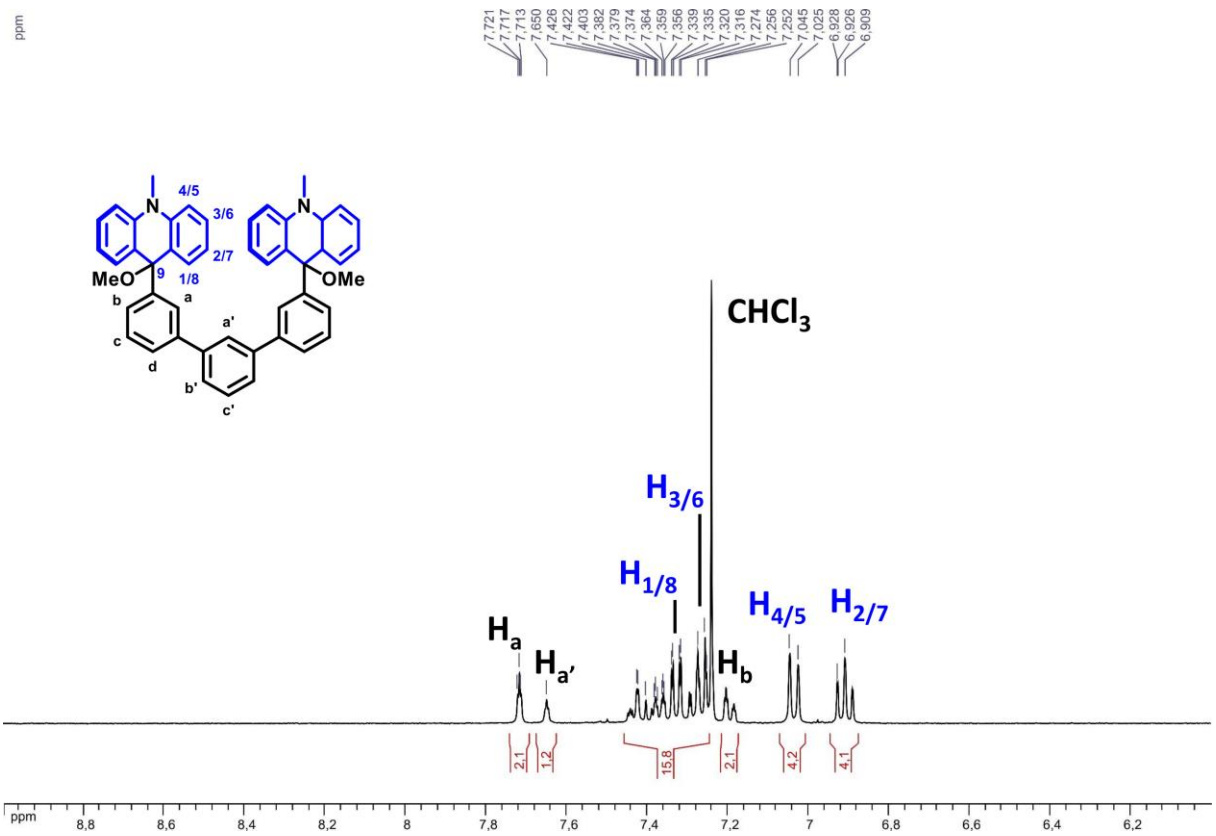

Figure S3.33: ^{1}H NMR (400 MHz, $CDCl_3$, 298 K) spectrum of **4** (aromatic region).

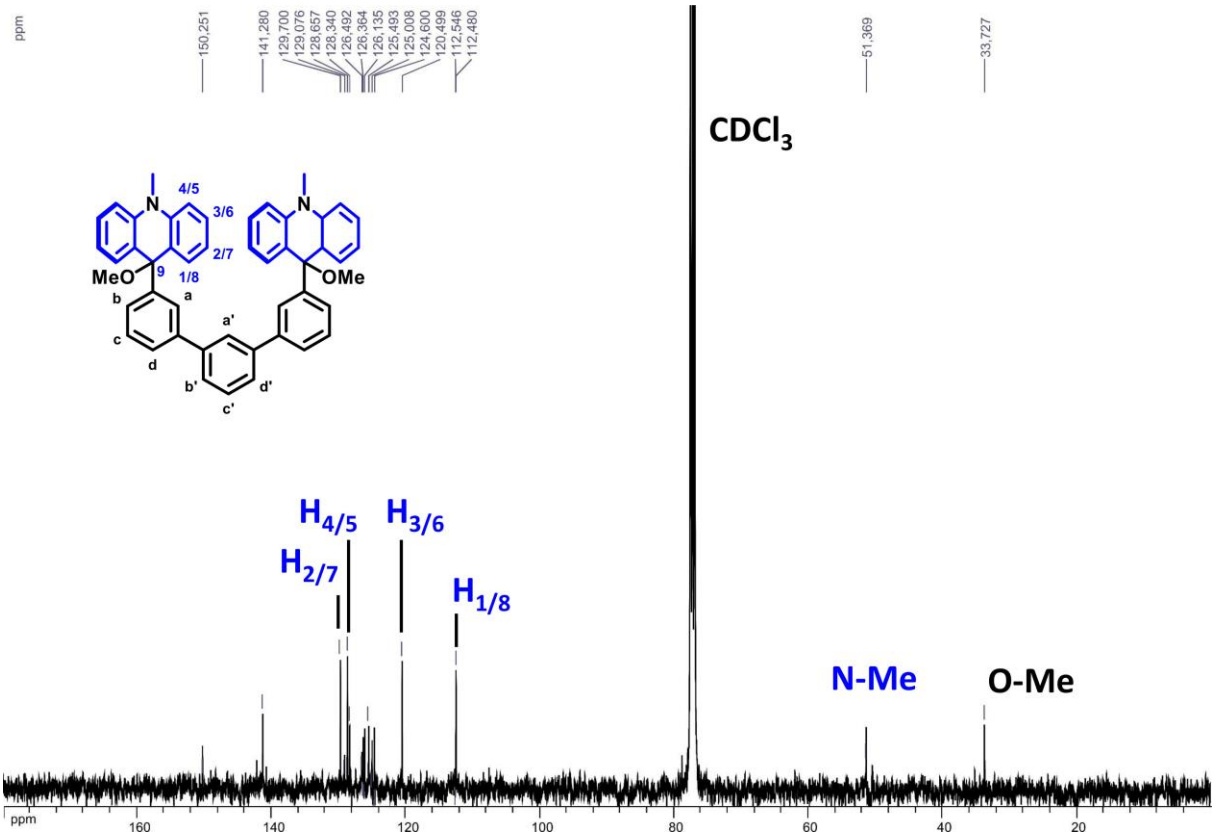

Figure S3.34: ^{13}C NMR (100 MHz, $CDCl_3$, 298 K) spectrum of **4**.

4. NMR Titration & Host-Guest Complex Formation

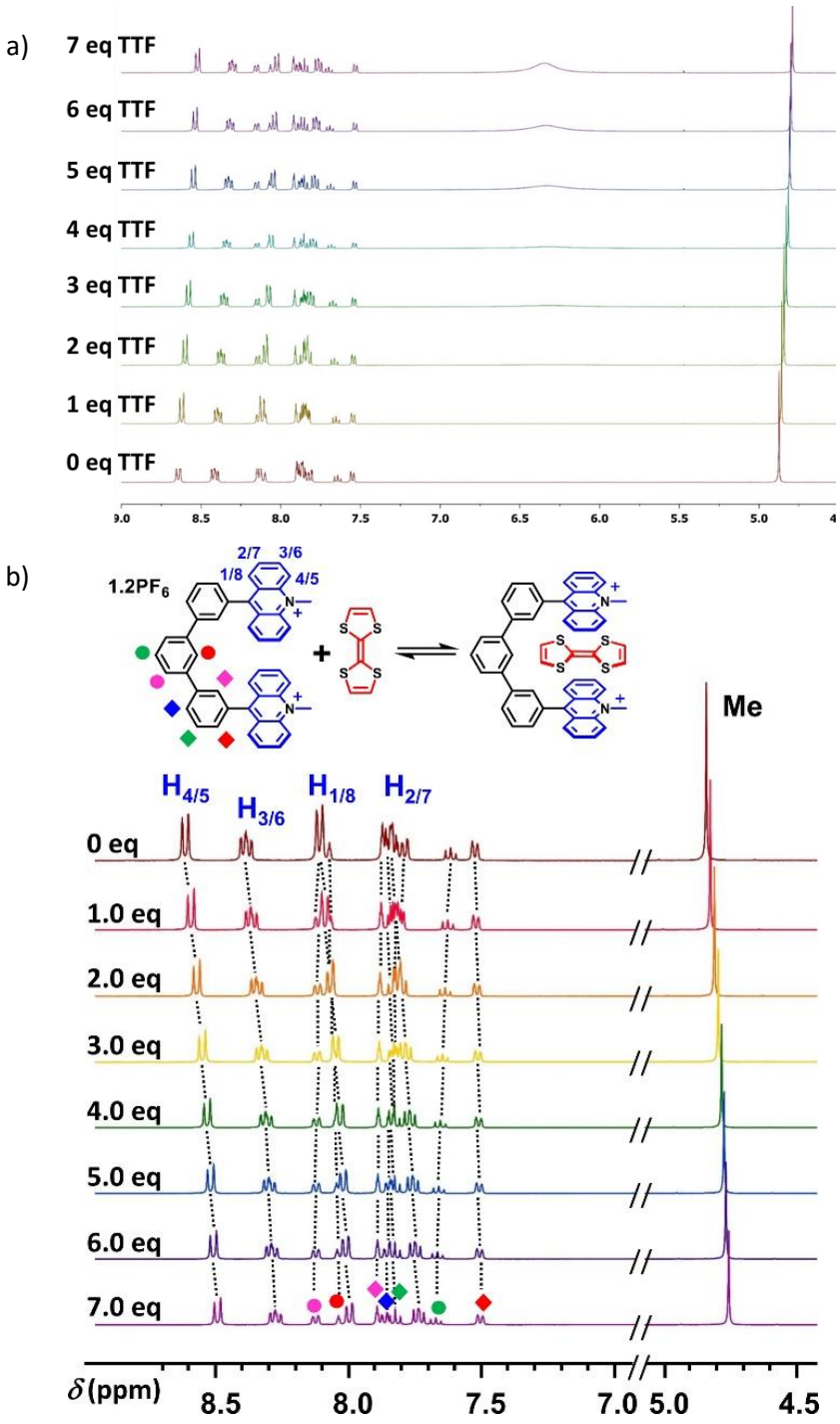

Figure S4.1: ^{1}H NMR (400 MHz, CD_3CN, 298 K) titration spectra revealing an upfield shift of the acridinic protons upon addition of small aliquots of a stock solution of TTF (c = 1.5.10^{-1} M) in $CDCl_3$ to a solution of **1.2PF6** (c = 10^{-2} M) in CD_3CN. Spectra recorded with 0, 1, 2, 3, 4, 5, 6 and 7 equiv. of TTF.

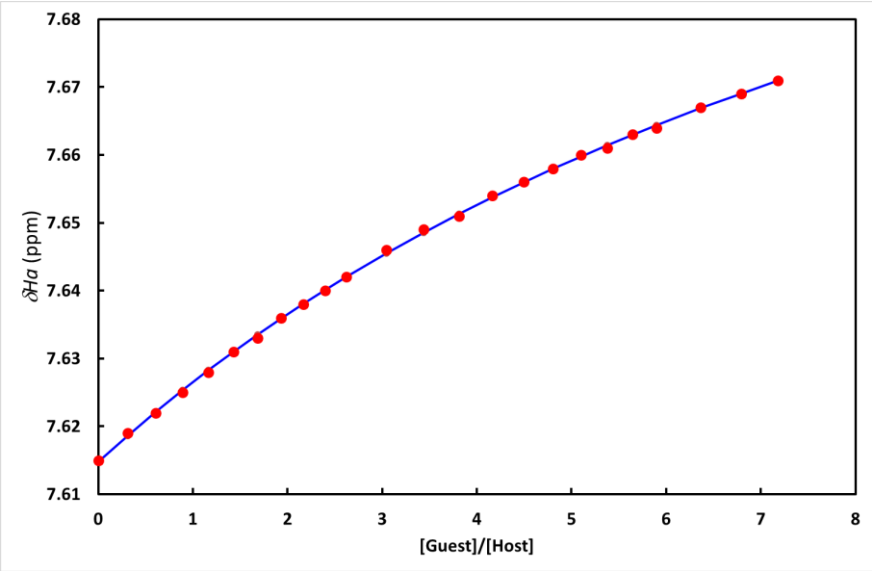

Figure S4.2: Change of the chemical shift of the $H_{c'}$ proton of **1.2PF$_6$** upon addition of TTF with the corresponding fitting to a 1:1 binding model.

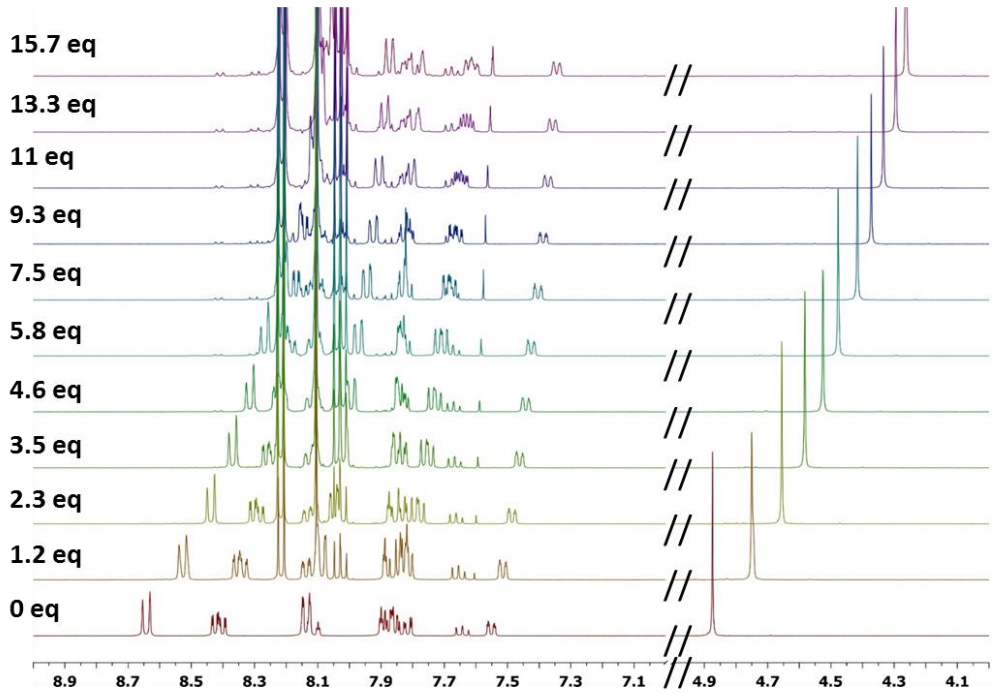

Figure S4.3: ^{1}H NMR (400 MHz, CD_3CN, 298 K) titration spectra revealing an upfield shift of the acridinic protons upon addition of small aliquots of a stock solution of pyrene (c = 3.10^{-1} M) in $CDCl_3$ to a solution of **1.2PF$_6$** (c = 10^{-2} M) in CD_3CN. Spectra recorded with 0, 1.2, 2.3, 3.5, 4.6, 5.8, 7.5, 9.3, 11, 13.3 and 15.7 equiv. of pyrene.

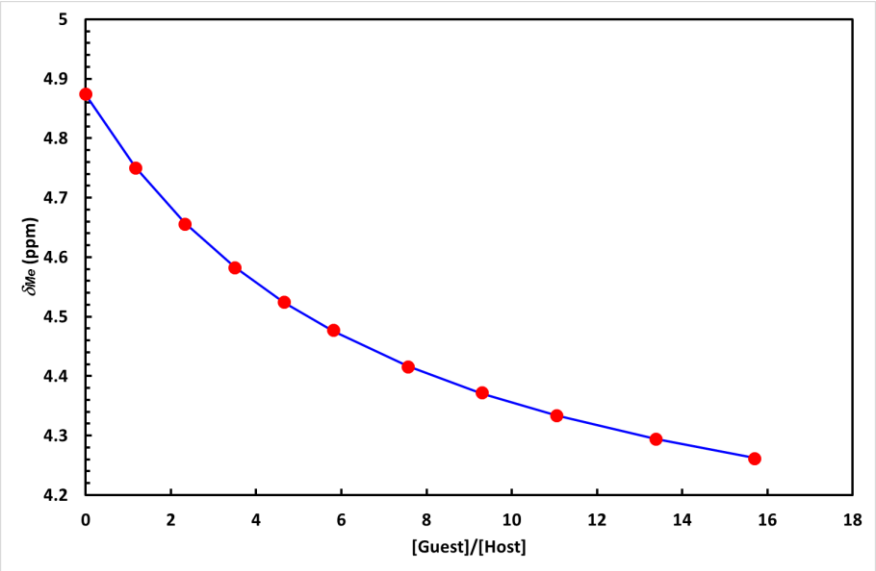

Figure S4.4: Change of the chemical shift of the *N*-methyl proton of **1.2PF6** upon addition of pyrene with the corresponding fitting to a 1:1 binding model.

5. UV-Vis Characterization of 1.2PF6

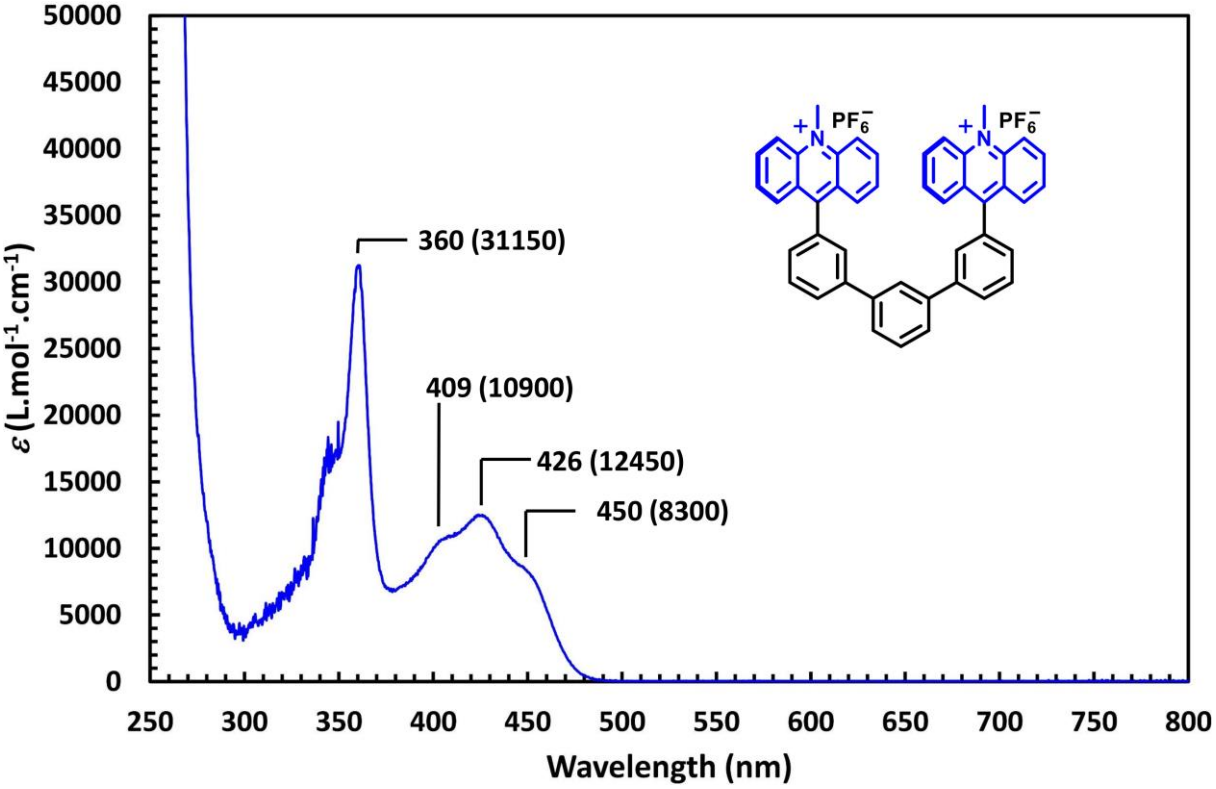

Figure S5.1: UV-Vis spectrum of **1.2PF6** (CH_3CN, $c = 5.10^{-5}$ M, $l = 1$ cm).

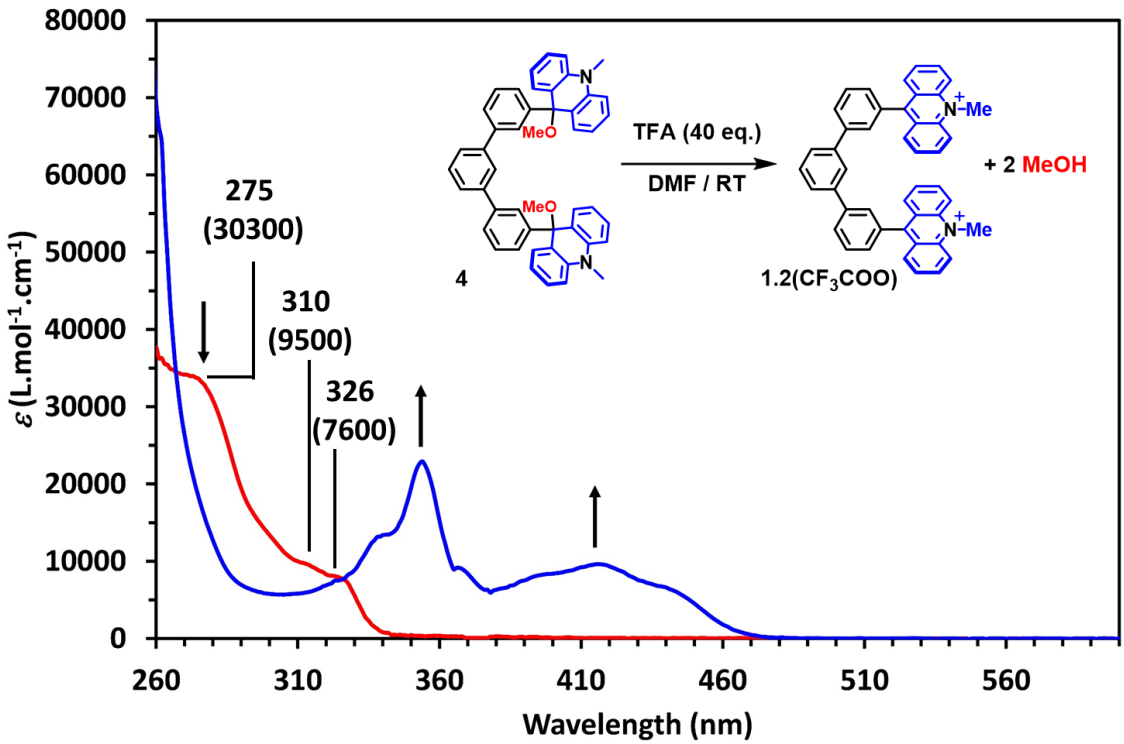

Figure S5.2: UV-Vis spectra of a solution of **4** (DMF, c = 4.10^{-5} M, l = 1 cm) before (**red**) and after addition of excess of TFA (**blue**).

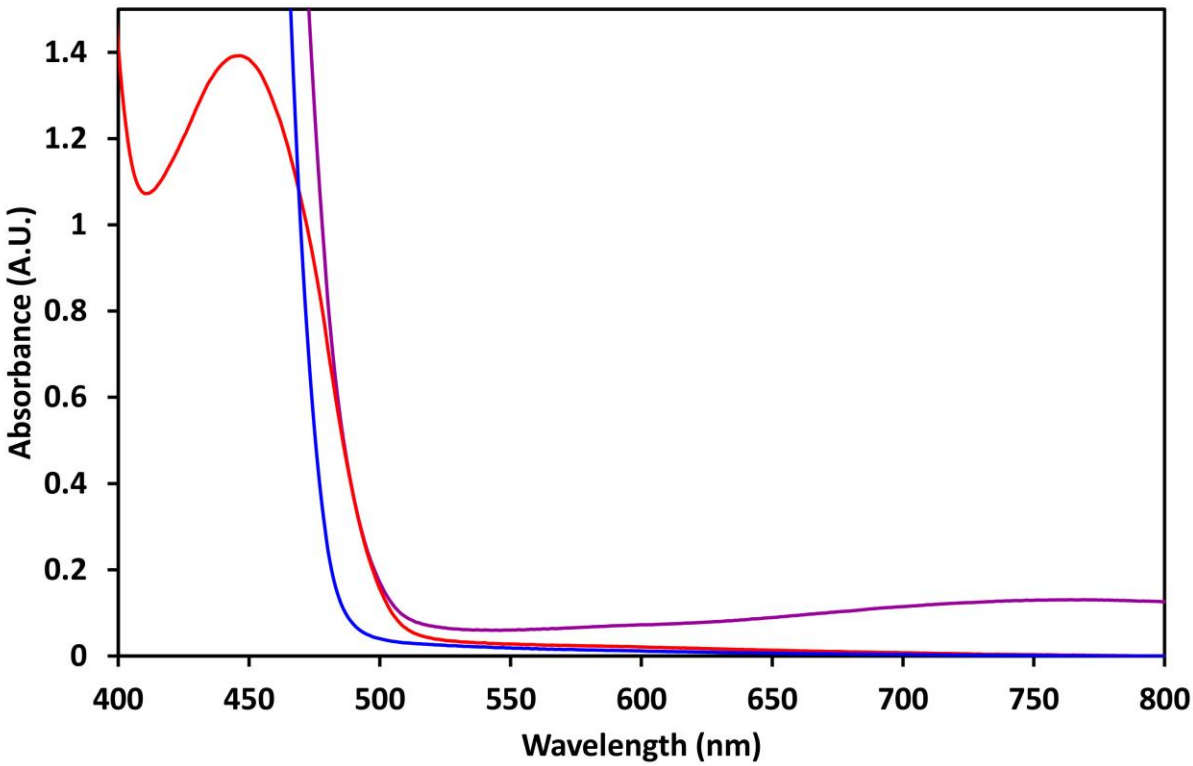

Figure S5.3: UV-Vis spectrum (CH_3CN, l = 0.1 cm) of **1.2PF$_6$** (blue, c = 5.10^{-3}M), TTF (red, c = 1.10^{-1} M) and **1.2PF$_6$** (c = 5.10^{-3}M) with 20 equiv. of TTF (purple).

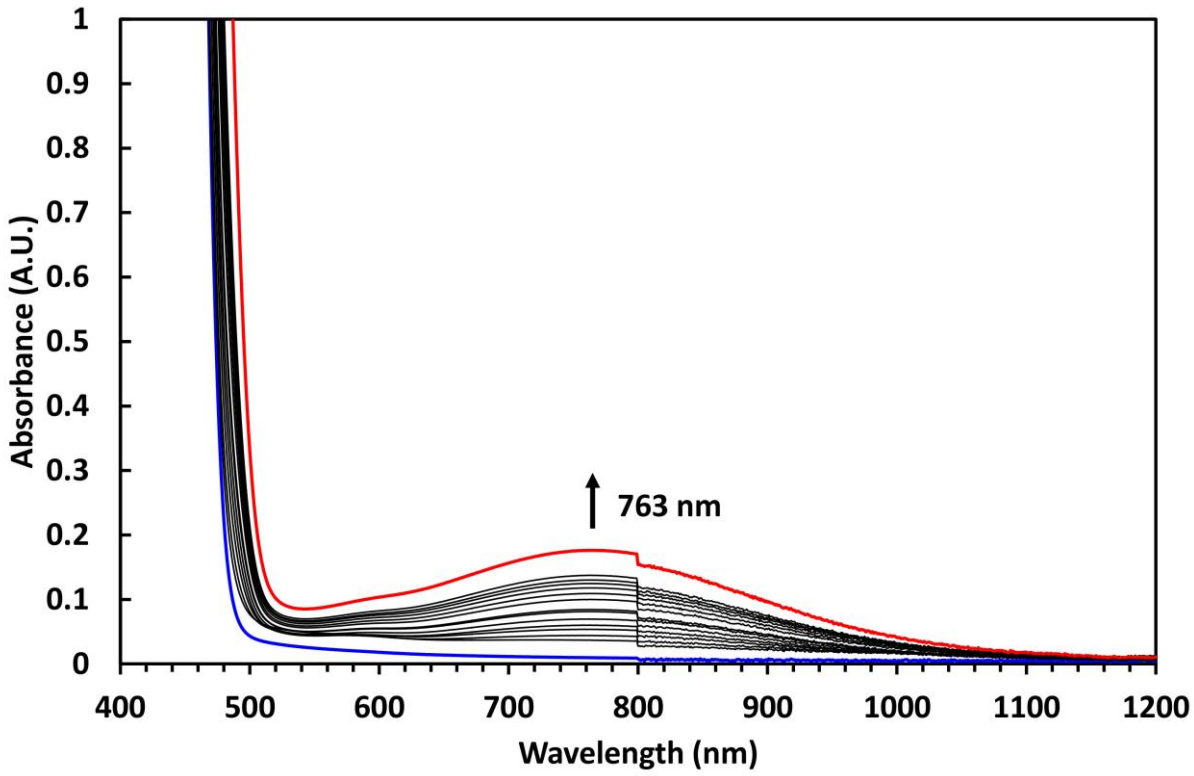

Figure S5.4: UV-Vis spectrum of **1.2PF$_6$** (CH_3CN, c = 5.10^{-3} M, l = 0.1 cm) upon addition of small aliquots of a stock solution of TTF (c = 1.10^{-1} M) in CH_3CN. Spectra recorded with 1, 2, 3, 4, 5, 6, 7, 8, 9, 10, 11, 12, 20 equiv. of TTF.

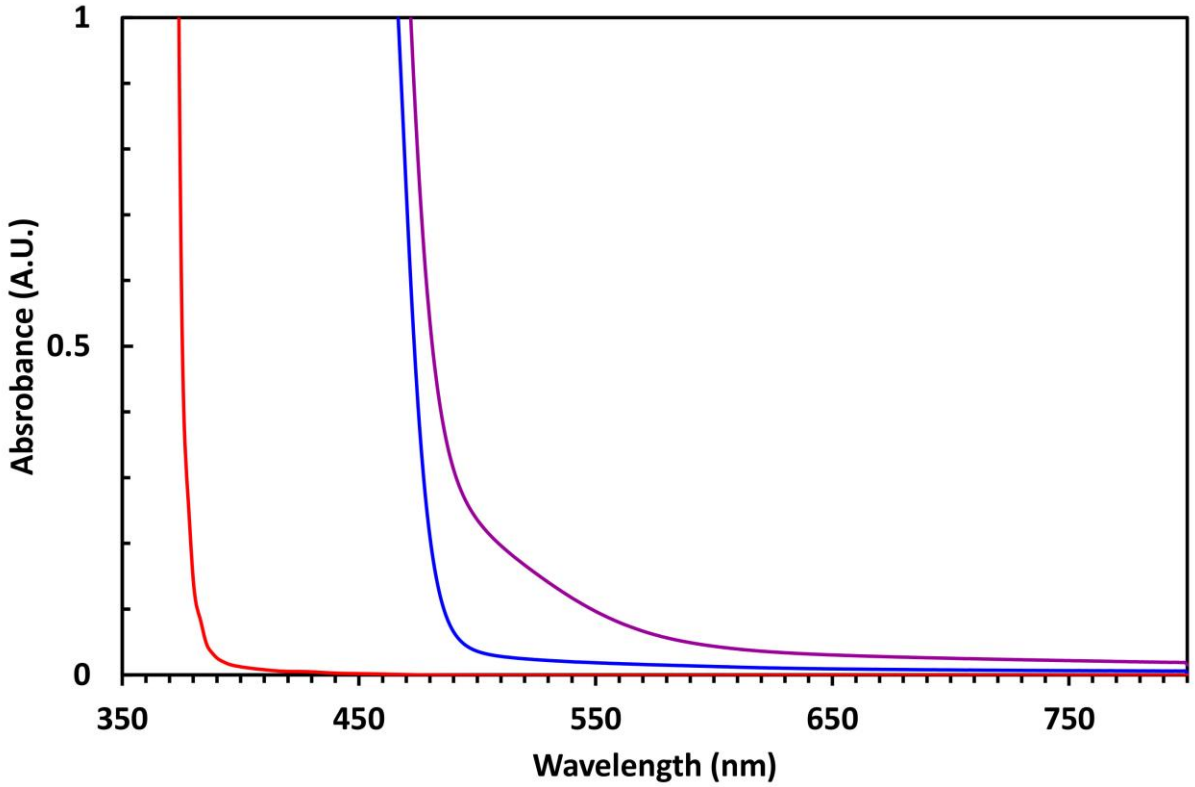

Figure S5.5: UV-Vis spectrum (CH_3CN, l = 0.1 cm) of **1.2PF$_6$** (blue, c = 5.10^{-3}M), pyrene (red, c = 1.10^{-1} M) and **1.2PF$_6$** (c = 5.10^{-3}M) with 20 equiv. of pyrene (purple).

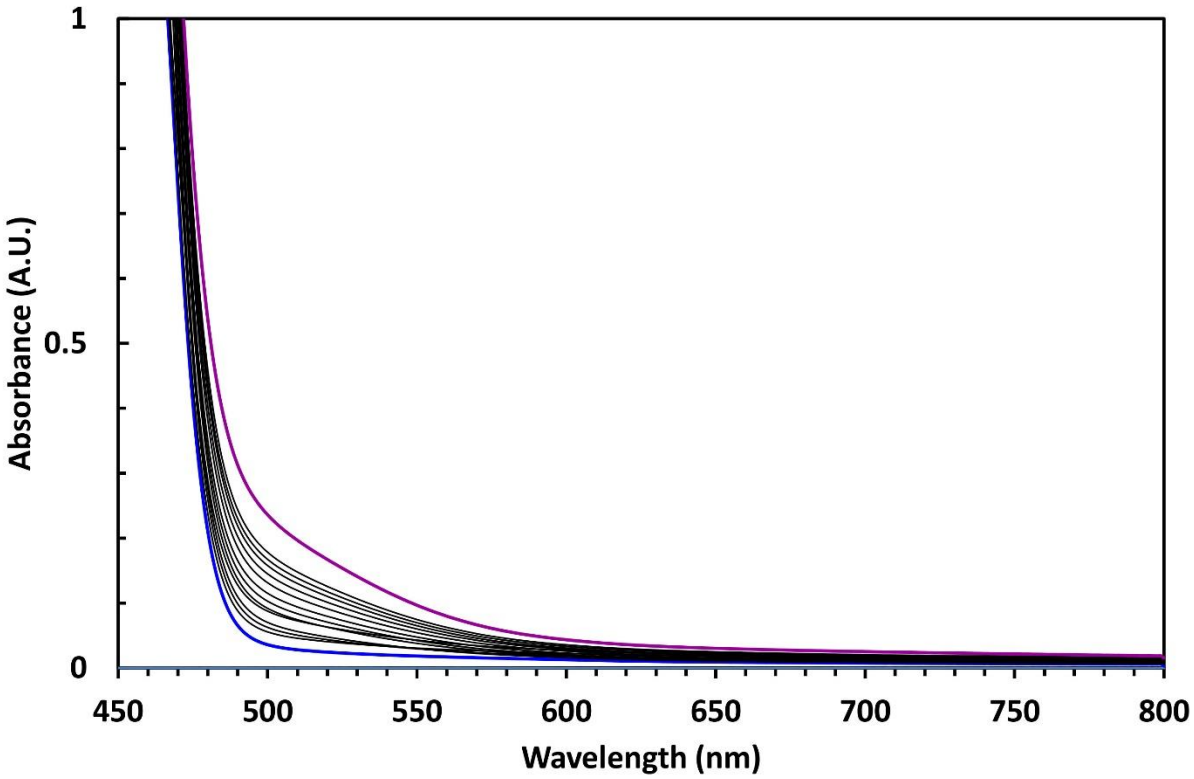

Figure S5.6: UV-Vis spectrum of **1.2PF6** (CH_3CN, $c = 5.10^{-3}$ M, $l = 0.1$ cm) upon addition of small aliquots of a stock solution of pyrene ($c = 1.10^{-1}$ M) in CH_3CN. Spectra recorded with 1, 2, 3, 4, 5, 6, 7, 8, 9, 10, 11, 12, 20 equiv. of pyrene

6. DFT Calculations

Table S6.1: Optimized conformations of $\mathbf{1}^{2+}$ obtained at the ωB97xD/6-31G(d) level of calculations.

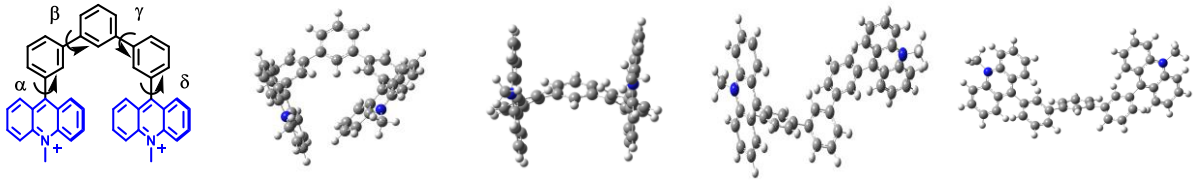

	T-Shape	**U**-Shape	**S**-Shape	**W**-Shape
E_{rel} (kJ/mol)	0	10.3	10.0	11.3
α (°)	90	74	74	73
β (°)	34	38	42	136
γ (°)	–40	–42	140	–136
δ (°)	62	74	74	72

Table S6.2: The calculated absorption energies (λ in nm) for the receptor $\mathbf{1}^{2+}$ at different DFT functionals using 6-31G* basis set in water medium.

Functional	$S_0 \rightarrow S_1$				$S_0 \rightarrow S_2$			
	λ_{calc} (nm)	λ_{exptl}[a] (nm)	Δ[b](nm)	f[c]	λ_{calc} (nm)	λ_{exptl}[a] (nm)	Δ[b](nm)	f[c]
PBE0	413	424	–11	0.148	363	361	0	0.025
BLYP	494		70	0.119	488		125	0.001
CAM-B3LYP	373		–51	0.170	311		–52	0.193
HSEH1PBE	420		–4	0.149	373		10	0.007
LC-ωPBE	338		–86	0.202	299		–64	0.292
ωB97xD	371		–53	0.168	309		–54	0.276
M06	419		–5	0.149	367		4	0.029
M062X	375		–49	0.183	312		–51	0.062

[a] taken from S. A. Jonker, F. Ariese and J. W. Verhoeven Red. Trav. Chim. Pays-Bas 1989**,** 108, 109-115. [b]$\Delta=\lambda_{calc}-\lambda_{exptl}$ [c]f: oscillator strength

$\mathbf{1}^{2+}$
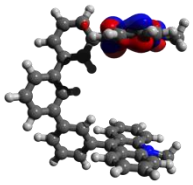
L+1
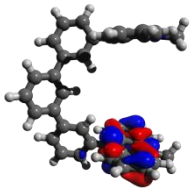
L
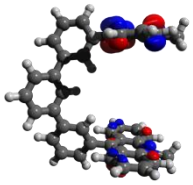
H-2
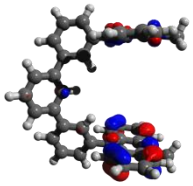
H-3
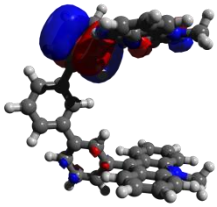
H-4
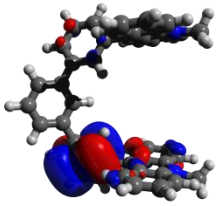
H-5

Figure S6.1: Isodensity plots of selected frontier molecular orbitals of the native $\mathbf{1}^{2+}$ and the direduced $\mathbf{1}^{0}$. The calculations were performed by M06/6-31G(d) level of theory and the isovalue is 0.02 a.u.

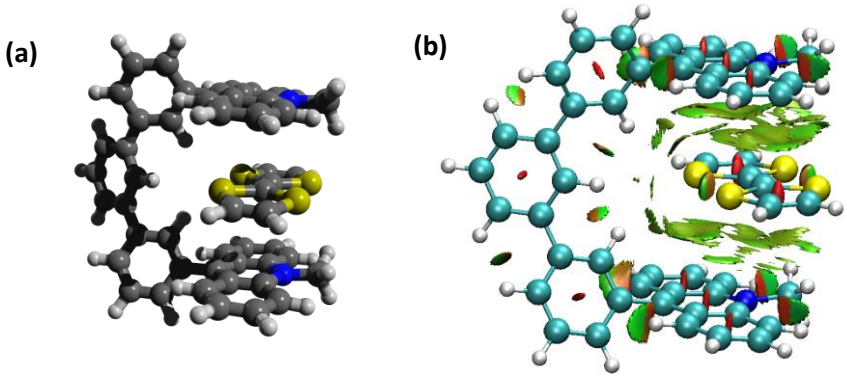

Figure S6.2: (a) Optimized geometry and (b) NCI isosurfaces (strong attractive interactions are represented in blue, weak interactions in green, and repulsive interactions in red, gradient isosurface s=0.5 a.u.) of TTF⊂1^{2+} inclusion complex

The regions in 3D space where weak intermolecular interactions occur in a complex can be displayed using the non-covalent index method (NCI) [S6]. This method is based on the analysis of the evolution of electron densities *ρ(r)* and their reduced gradients, *s(r)*. Regions with low electron density *ρ(r)* and reduced density gradient *s(r)* correspond to the occurrence of noncovalent interactions. Using NCI index, different regions of weak interactions can be identified by color. Blue regions correspond to stronger attractive interaction such as established in hydrogen bond. The interaction marked by green color can be identified as Van der Waals interaction region. Finally the regions showing strong steric effect are colored in red. Color filled isosurfaces graphs were calculated using the Multiwfn[S7] and have been plotted using VMD programs[S8]. The gradient isosurfaces filling the interlayer space between TTF and acridylium moieties suggest π-π stacking interaction between aromatic units.

7. Single Crystal X-Ray Crystallographic Information

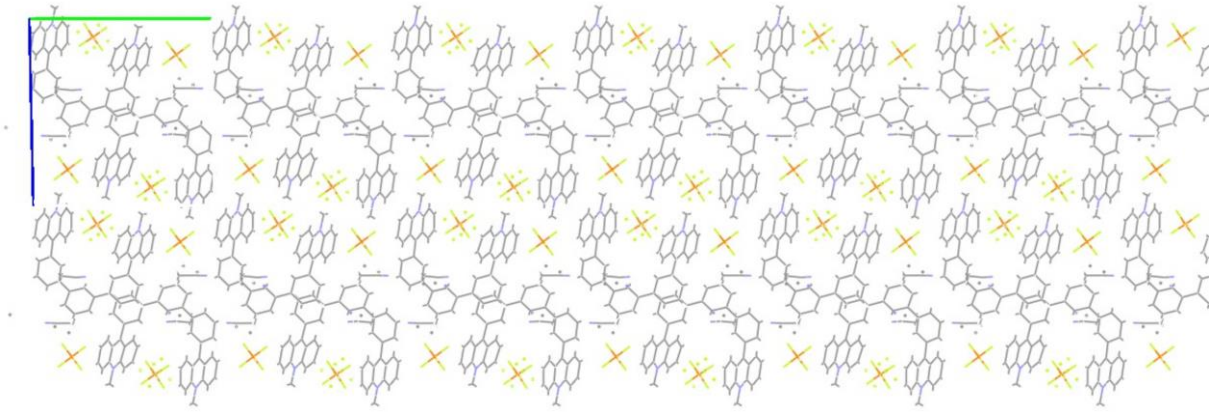

Figure S7.1: Representation of the crystal packing along the *a* axis.

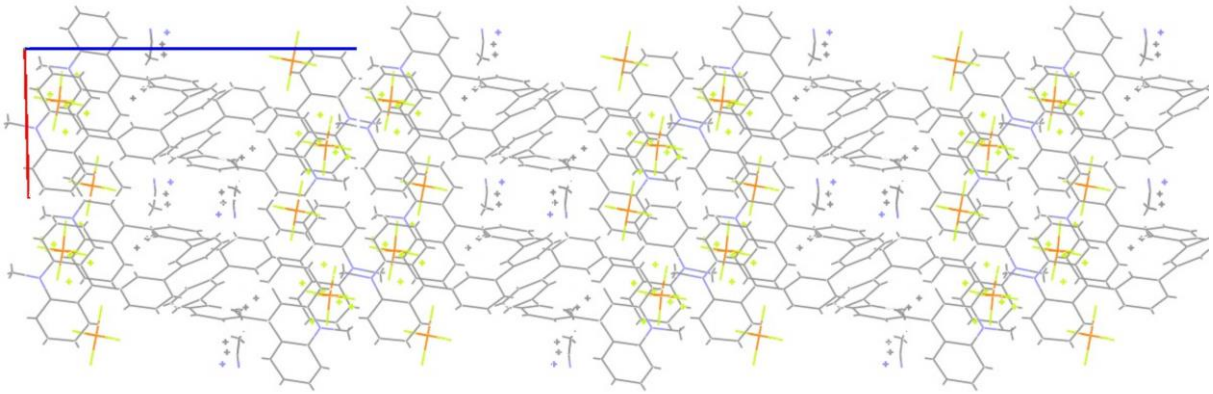

Figure S7.2: Representation of the crystal packing along the *b* axis.

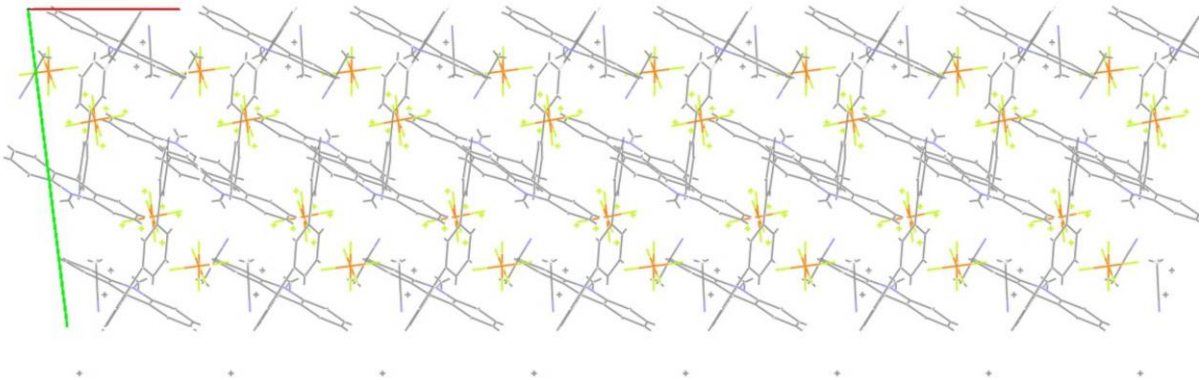

Figure S7.3: Representation of the crystal packing along the *c* axis.

8. References

[S1] Luca A. Andronico, Arianna Quintavalla, Marco Lombardo, Mara Mirasoli, Massimo Guardigli, Claudio Trombini, and Aldo Roda *Chem. Eur. J.*, **2016**, *22*, 18156–18168.

[S2] Han F. S., Higuchi M., and Kurth D. G. *Org. Lett.*, **2007**, *9* (4), 559–562.

[S3] L. J. Farrugia, *Journal of App. Cryst.* **1999**, *32*, 837–838.

[S4] G. M. Sheldrick, *Acta Cryst., Section A* **2015**, *71*, 3–8.

[S5] G. M. Sheldrick, *Acta Cryst., Section C* **2015**, *71*, 3–8.

[S6] a) E. R. Johnson, S. Keinan, P. Mori-Sanchez, J. Contreras-Garcia, A. J. Cohen, W. Yang, *J. Am. Chem. Soc.* **2010**, *132*, 6498–6506; b) J. Contreras-Garcia, E. R. Johnson, S. Keinan, R. Chaudret, J.-P. Piquemal, D. N. Beratan, W. Yang *J. Chem. Theory. Comput.* **2011**, *7*, 625.

[S7] Tian Lu, Feiwu Chen, Multiwfn: A Multifunctional Wavefunction Analyzer, *J. Comp. Chem.* **2012**, *33*, 580-592.

[S8] W. Humphrey, A. Dalke A, K. Schulten, *J. Mol. Graphics* **1996**, *14*, 33.